END

DATE
FILMED

1-8

DTIC

MICROCOPY RESOLUTION TEST CHART
NATIONAL BUREAU OF STANDARDS-1963-A

LEVEL (12) (18) (19)

DNA 4826F

AD A091806

(6)

AN ANALYSIS OF THE CHARACTERISTICS OF RAYLEIGH WAVES PRODUCED BY SURFACE EXPLOSIONS.

Computer Sciences Corporation
6565 Arlington Boulevard
Falls Church, Virginia 22046

(11) 31 January 1979   (12) 28   (10) J. R. Murphy

(9) Final Report. 5 July 77—31 Jan 79,

CONTRACT No. DNA 001-77-C-0272

(15)

APPROVED FOR PUBLIC RELEASE;
DISTRIBUTION UNLIMITED.

DTIC
SELECTED
NOV 18 1980

A

(16)   (17) B249|

DDC FILE COPY

Prepared for
Director
DEFENSE NUCLEAR AGENCY
Washington, D. C. 20305

8011 14 021

REPORT DOCUMENTATION PAGE	READ INSTRUCTIONS BEFORE COMPLETING FORM	
1. REPORT NUMBER DNA 4826F V	2. GOVT ACCESSION NO. AD-A091 806	3. RECIPIENT'S CATALOG NUMBER
4. TITLE (and Subtitle) AN ANALYSIS OF THE CHARACTERISTICS OF RAYLEIGH WAVES PRODUCED BY SURFACE EXPLOSIONS		5. TYPE OF REPORT & PERIOD COVERED Final Report for Period 5 Jul 77 - 31 Jan 79
		6. PERFORMING ORG. REPORT NUMBER
7. AUTHOR(s) J. R. Murphy		8. CONTRACT OR GRANT NUMBER(s) DNA 001-77-C-0272
9. PERFORMING ORGANIZATION NAME AND ADDRESS Computer Sciences Corporation 6565 Arlington Boulevard Falls Church, VA. 22046		10. PROGRAM ELEMENT, PROJECT, TASK AREA & WORK UNIT NUMBERS Subtask Y99QAXSB049-12
11. CONTROLLING OFFICE NAME AND ADDRESS Director Defense Nuclear Agency Washington, D.C. 20305		12. REPORT DATE 31 January 1979
		13. NUMBER OF PAGES 80
14. MONITORING AGENCY NAME & ADDRESS(if different from Controlling Office)		15. SECURITY CLASS. (of this report) UNCLASSIFIED
		15a. DECLASSIFICATION/DOWNGRADING SCHEDULE

16. DISTRIBUTION STATEMENT (of this Report)

Approved for public release; distribution unlimited.

17. DISTRIBUTION STATEMENT (of the abstract entered in Block 20, if different from Report)

19. KEY WORDS (Continue on reverse side if necessary and identify by block number)

Seismology
Ground Motion
Underground Nuclear Explosions
Ground Roll
Valley Reverberation

20. ABSTRACT (Continue on reverse side if necessary and identify by block number)

The successful deployment of an MX missile system requires a careful considera-tion of ground shock effects which were of secondary importance in previous ap-plications. For example, with the system sited in a valley and under a multiple attack scenario, untargeted points can be expected to experience a significant ground motion environment as a result of the superposition of motions originating from attacks on a variety of surrounding aimpoints. Furthermore, reflections of outgoing energy from the valley boundaries can be expected to complicate the ground motion environment within the valley, particularly at late times. The

20. Abstract (Continued)

objective of the work described in this report has been to develop a better
quantitative understanding of these late-time, long-period ground motions in
order to provide a firmer basis for scaling to new geologic conditions. Par-
ticular emphasis has been placed on the identification of the characteristic
mode of propagation associated with these arrivals. A theoretical model is
described which has been used to compute the surface waves produced by a prop-
agating airblast load acting on the surface of a multilayered, elastic half-
space. This model was then applied to the analyses of both the observed data
and finite difference simulations of the Pre-Mine Throw and Pre-Dice Throw 100
ton HE surface blasts. In addition, a preliminary assessment has been made of
the influence of valley boundaries on the late-time ground motion environment
within the valley. Two sets of data recorded from underground nuclear tests
conducted at the Nevada Test Site were analyzed in an attempt to define the
source and relative amplitude of secondary arrivals originating from the inter-
action of the primary outgoing motion with the subsurface structural boundaries.

TABLE OF CONTENTS

LIST OF ILLUSTRATIONS

LIST OF ILLUSTRATIONS (Continued)

LIST OF ILLUSTRATIONS (Continued)

Chapter 1

Introduction

It is now apparent that the successful deployment of an MX system will require the careful consideration of effects which were clearly of secondary importance in previous applications. For example, with regard to the design ground motion environment, the clustered multiple protective structure concept together with the site requirements have combined to increase the relative importance of the late-time, longer-period ground motions associated with elastic wave propagation at the site. That is, the system will be sited in a valley and, under a multiple attack scenario, untargeted points can be expected to experience a significant ground motion environment as the result of the combination of motions originating from attacks on a variety of surrounding aim-points. Furthermore, reflections of outgoing energy from the valley boundaries can be expected to complicate the ground motion environment within the valley, particularly at late times.

The objective of the analyses described in this report has been to develop a better, quantitative understanding of these late-time, long-period ground motions in order to provide a firmer basis for scaling to new geologic conditions and source environments. During the past year particular emphasis has been placed on the identification of the characteristic mode of propagation associated with these arrivals and Chapter 2 summarizes the progress in this area. In this chapter, a theoretical model is described which can be used to compute the surface waves produced by a propagating airblast load acting on the surface of a multilayered, elastic halfspace. This model is then applied to the analyses of both the observed data and finite difference simulations of the Pre-Mine Throw and Pre-Dice Throw 100 ton HE surface blasts.

A preliminary assessment of the influence of the valley boundaries on the late-time ground motion environment within the valley is described in Chapter

3. Two sets of data recorded from underground nuclear tests conducted at the Nevada Test Site are analyzed in an attempt to define the source and relative amplitude of secondary arrivals originating from the interaction of the primary outgoing motion with the subsurface structural boundaries. This is followed in Chapter 4 by a summary and recommendations for further study.

Chapter 2

Rayleigh Waves From Surface Explosions

2.1   Introduction

It has frequently been observed that the ground motion records from surface explosions are significantly influenced by low frequency, oscillatory components which appear to have the characteristics of Rayleigh waves. This is found to be true even at relatively near-field distances where body waves and directly induced motions might be expected to dominate. The analyses described in this Chapter have been directed at an attempt to develop a clearer understanding of these data. The study was originally motivated by the observation that simulations of several 100 ton HE tests using a two-dimensional, elastic finite difference code gave results which agreed remarkably well with the observed ground motion data from these events, despite the fact that only the airblast component of the seismic loading was considered (Auld et al., 1978). This raised the possibility that it might be feasible to predict the low frequency component of the radiated elastic wave field from such explosions using simple approximations to the seismic source function. If this turns out to be the case, then once the mode of propagation associated with this component of the motion has been conclusively identified, its scaling as a function of yield and site geology can be guided by quantitative insight provided by elastic wave theory.

In the following sections the analytic solution to the problem of Rayleigh waves generated by an airblast acting on the surface of a multi-layered, elastic halfspace is described and then applied to the identification of surface wave components in the ground motion measured from several explosive tests.

2.2   Description of the Model

The problem under investigation concerns the elastic response of
a multilayered halfspace to an axisymmetric normal load acting on the surface
(i.e., an approximation to an airblast). The geometry of the problem is
illustrated in Figure 2-1 which shows a sequence of constant thickness (d_i)
layers overlying a semi-infinite halfspace excited by a source centered at
the origin. As a first approximation, the layers are taken to be perfectly
elastic and are characterized by their Lamé constants (λ, μ) and density (ρ).
In principle, this problem can be solved either numerically or analytically
and each approach has its advantages and disadvantages. The numerical approach,
as exemplified by the finite difference procedure, has the advantage that
the complete response can be computed at any designated target point. The
associated disadvantages are: (1) that the solution provides no explicit
information concerning which arrivals (i.e., P, S or surface waves) are
dominating the motion at any given time and (2) that it becomes progressively
more expensive to compute the motion at large distances and late times. On
the other hand, the analytic approach has the advantage that the contributions
due to different wave arrivals can be easily identified and computed separately,
thereby providing some physical insight into the problem. The disadvantage
in this case is that the analytic solution representing the complete
response of the multilayered halfspace is very complicated and not yet fully
developed. Fortunately, however, the surface wave portion of the problem is
simple enough that the exact solution can be written down using the matrix
formulation of the boundary value problem pioneered by Haskell (1953) and
Harkrider (1964). This solution is outlined below.

It can be shown (e.g., Ewing, et al., 1957, Chapter 4) that the
Fourier transform of the vertical (W) and radial (U) displacement due to all
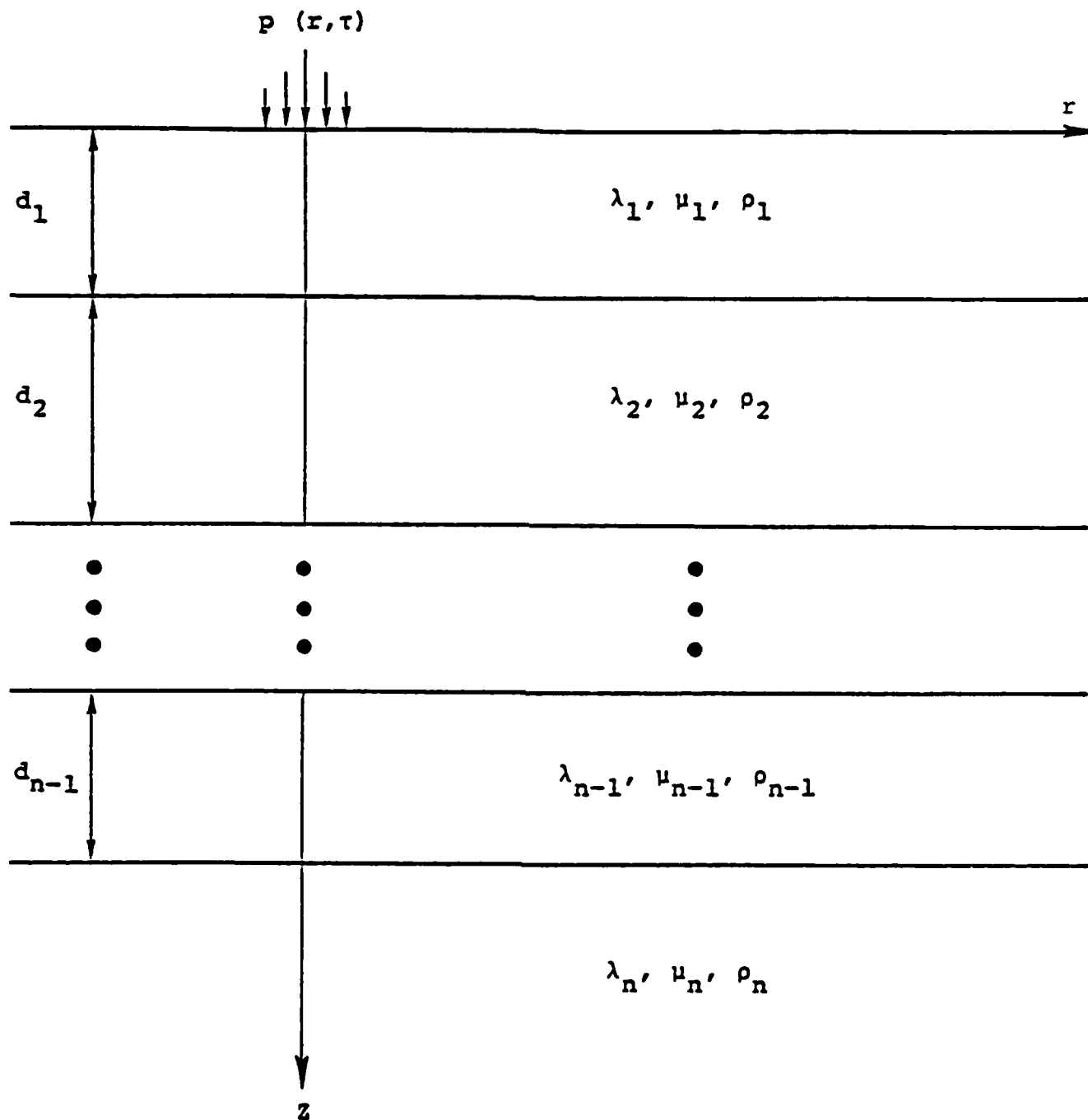
Figure 2-1: Multilayered Elastic Halfspace Loaded by an Axisymmetric Surface Overpressure

wave arrivals can be written as an integral over wave number k of the form

$$W, U = \int \frac{Q(\omega,k,r)}{F_R(\omega,k)} \, dk \tag{2-1}$$

where Q and F_R are complex functions of k and the angular frequency ω whose explicit form depends upon the boundary conditions to the problem. Now it can be shown that the condition

$$F_R(\omega,k) = 0 \tag{2-2}$$

which specifies the poles of the integrand in Equation (2-1), corresponds to the Rayleigh wave dispersion equation and consequently the residue contributions to the integral (Equation 2-1) give the surface waves. It follows that the Rayleigh wave contribution to the motion for mode j is given by

$$W_{R_j}, U_{R_j} = 2\pi i \frac{Q(\omega,k_j,r)}{\left(\frac{\partial F_R}{\partial k}\right)_j} \tag{2-3}$$

where Q and $(\partial F_R / \partial k)_j$ are evaluated at (ω, k_j) such that $F_R(\omega,k_j) = 0$. Harkrider, et al., (1974) have shown that for airblast loading conditions, the solution (Equation 2-3) has an explicit representation in the form

$$W_{R_j}(\omega,r) = -i\pi A_{R_j} H_0^{(2)}(k_j r) S_j(\omega) \tag{2-4}$$

$$U_{R_j}(\omega,r) = \xi_j(\omega) \frac{H_1^{(2)}(k_j r)}{H_0^{(2)}(k_j r)} W_{R_j}(\omega,r)$$

where A_{R_j} is the Raleigh wave site response function, $H_i^{(2)}(k_j r)$ is the Hankel function propagation term $(i = o,1)$, ξ_j is the ellipticity, and $S_j(\omega)$ is the Raleigh wave source function given by

$$S_j(\omega) = \int_{r_1}^{r_2} p(r',\omega) \, J_0(k_j r') \, r' \, dr' \qquad (2\text{-}5)$$

where $p(r',\omega)$ is the Fourier transform of the airblast load acting over the surface disk extending from r_1 to r_2 and $J_0(k_j r')$ is the Bessel function kernel.

Equations (2-4) and (2-5) give the Fourier transform of the Rayleigh wave displacement in mode j due to an arbitrary airblast loading function $p(r,t)$ acting on the free surface $z = 0$. The corresponding time domain displacements can be obtained from this solution using a simple numerical Fourier inversion of the computed frequency domain solution.

2.3   Applications to the Pre-Mine Throw and Pre-Dice Throw Experiments

In this section the analytic surface wave model described above will be applied to the analysis of the ground motion data measured from the Pre-Mine Throw and Pre-Dice Throw experiments.

2.3.1 General Description of the Experiments

The Pre-Mine Throw (PMT) and Pre-Dice Throw (PDT) experiments were both 100 ton HE surface bursts conducted at the Nevada Test Site (NTS) and White Sands Missile Range respectively. The principal difference between the two sites is that the PMT site is classified as "dry" whereas the PDT site is classified as "wet". That is, the soil at depths below a few feet at the PDT site is saturated while the soil at the PMT site is dry. Approximate subsurface geologic profiles for the two sites are shown in Figure 2-2. In this figure, α and β denote the compressional and shear wave velocities respectively and the hatch marks at the bottom of the sections indicate that the material below this depth was treated as rigid in the finite difference analysis of the problem. This condition has been

13
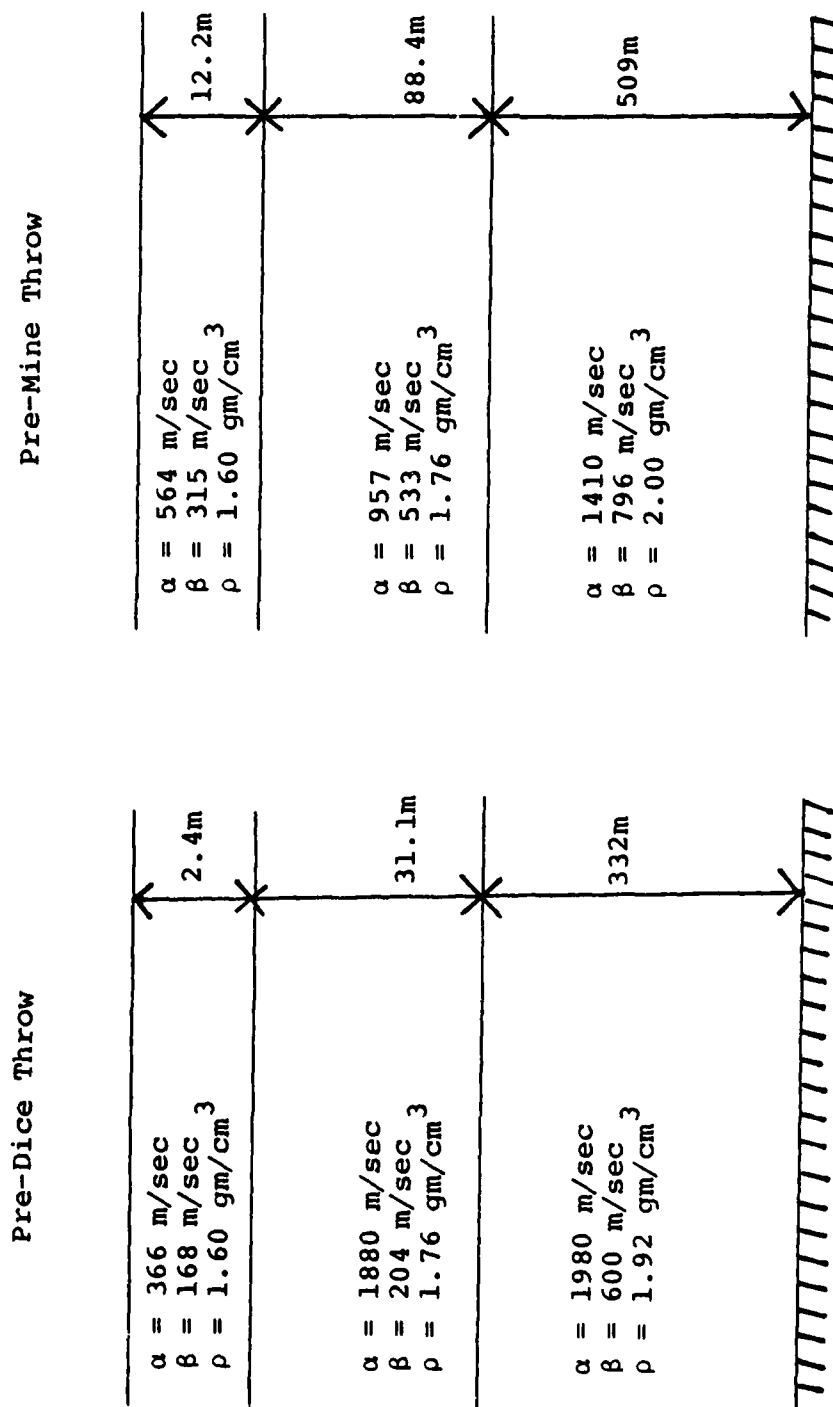
Figure 2-2. Approximate Subsurface Geologic Models for Pre-Dice Throw and Pre-Mine Throw.

14

approximated in the analytic solution by assigning values of $\alpha = 10,000$ m/sec and $\beta = 6,000$ m/sec to the halfspace extending below this depth. Comparing the two sections shown in this figure, it can be seen that the PDT site is characterized by an approximately 30m thick near-surface layer in which the shear wave velocity is relatively low with respect to the corresponding PMT value and Poisson's ratio is nearly 0.5 indicating that the material is water saturated.

The theoretical fundamental mode Rayleigh wave dispersion curves for the two sites are shown in Figure 2-3. It can be seen that over the frequency range of interest the Rayleigh wave propagation velocities predicted for the PDT site are significantly lower than those predicted for the PMT site, consistent with the differences in the shear wave velocity profiles noted above. Moreover, the group velocity curve for the PDT site is characterized by a single pronounced group velocity minimum as opposed to that for the PMT site which shows at least two relatively shallow group velocity minima. It will be shown later in this section that these differences correlate with a fundamental mode Rayleigh wave signal for the PDT site which is quite narrowband relative to that for the PMT site. The theoretical fundamental mode Rayleigh wave site response functions (A_r) for PDT and PMT are compared in Figure 2-4. It can be seen that in both cases the response drops off sharply for frequencies below about 2.0 Hz, indicating that the Rayleigh wave propagation at these sites can be expected to be dominated by relatively high frequency components. Above 2.0 Hz the PDT response is relatively flat whereas the PMT response shows evidence of a second corner frequency at about 10.0 Hz. Again, this is consistent with the differences in the effective bandwidth of the propagating Rayleigh waves at the two sites noted above in the comparison of the dispersion curves.
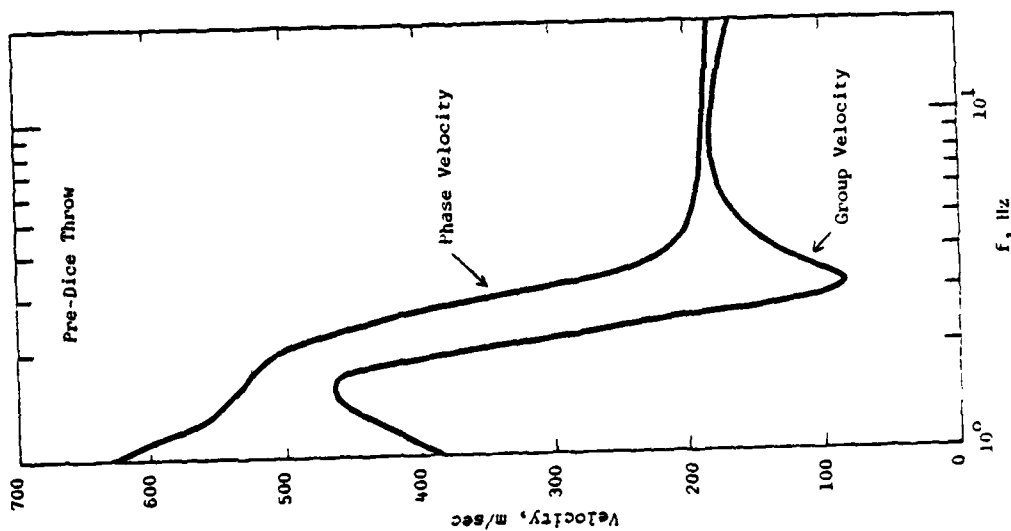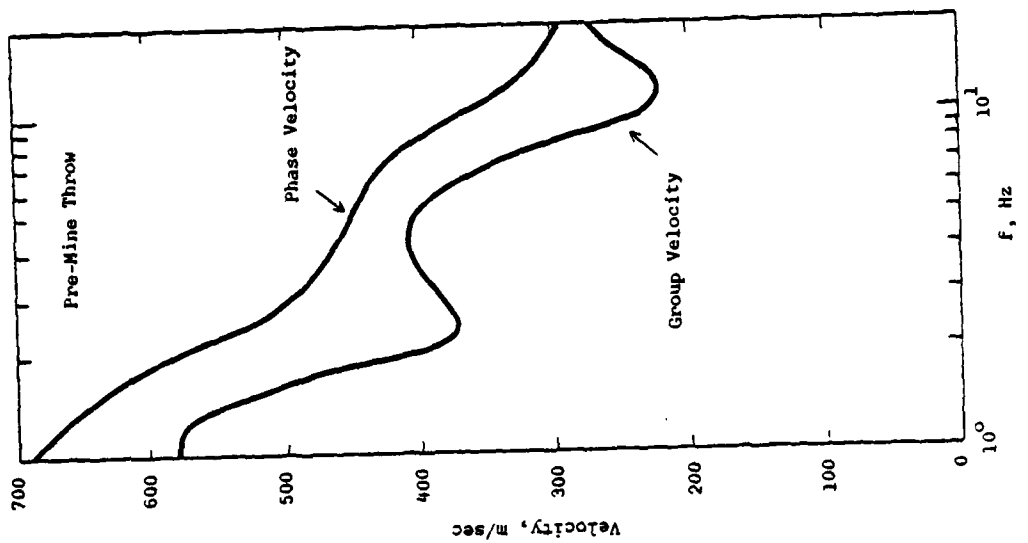
Figure 2-3: Comparison of Dispersion Curves for Pre-Dice and Pre-Mine Throw Sites

16
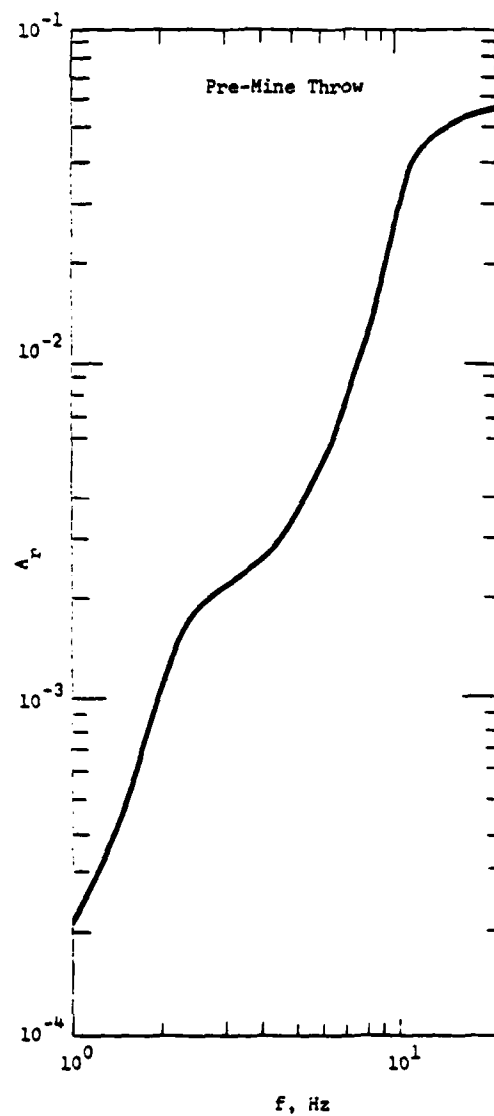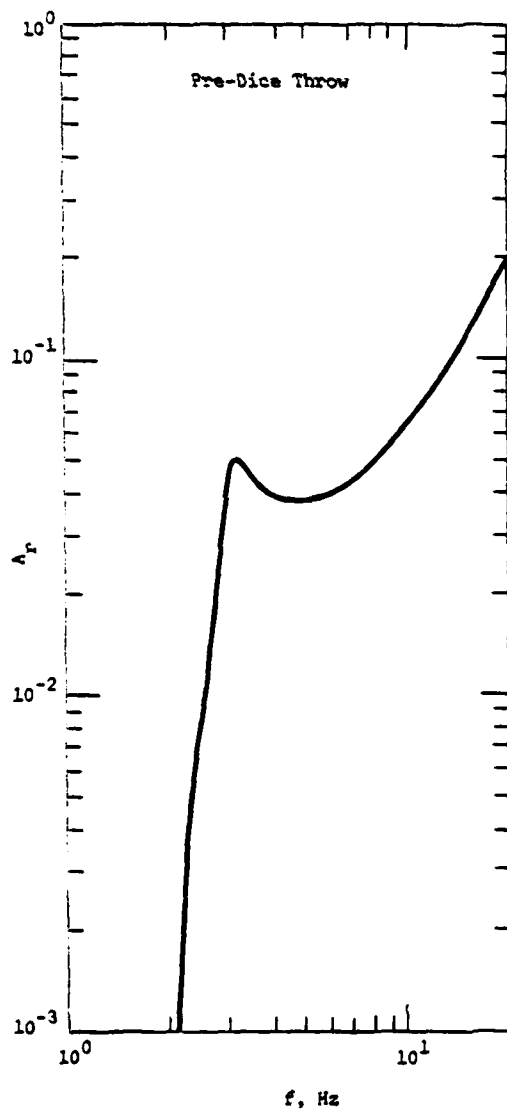
Figure 2-4: Comparison of Rayleigh Wave Site Response
Function (A_r) for Pre-Dice Throw and Pre-
Mine Throw Sites

17

In the following two sections the site models described above will be used in conjunction with an approximation to the airblast load to compute the expected Rayleigh wave contribution to the ground motion for PMT and PDT.

2.3.2. Pre-Mine Throw Rayleigh Wave Simulation

As an initial test of the analytic Rayleigh wave solution, a simple problem was analyzed in which the free surface of the PMT geologic model was loaded with a low frequency, propagating overpressure consisting of one-half cycle of a 2.0 Hz sine wave. The amplitude of the pressure pulse was taken to decay exponentially from a level of 1000 psi at a range of about 7.5m to a level of 1 psi at a range of about 300m. At ranges less than 7.5m the amplitude of the overpressure was held constant at 1000 psi. The pulse propagation velocity was taken to have a constant value of 457 m/sec over the entire range from 0 to 300m. Thus, the functional form of the Fourier transform of the assumed overpressure is

$$p(r,\omega) = C e^{-\alpha r} e^{-i\omega t_o} \hat{p}(\omega) \qquad (2\text{-}6)$$

where

$$t_o = r/c_o, \qquad c_o = 457\,\text{m/sec}$$
$$C = 1000\,\text{psi}, \qquad \alpha = 0, \qquad\qquad r \leq 7.5\,\text{m}$$
$$C = 1194\,\text{psi}, \qquad \alpha = 0.002\text{m}^{-1} \quad r \geq 7.5\,\text{m} \qquad (2\text{-}7)$$

and

$$\hat{p}(\omega) = \int_0^{\frac{T}{2}} \sin\frac{2\pi}{T}t\, e^{-i\omega t}\, dt = \frac{\omega_o(1 + \cos\frac{\omega T}{2}) - i\omega_o \sin\frac{\omega T}{2}}{\omega_o^2 - \omega^2} \qquad (2\text{-}8)$$

with $\omega_o = 2\pi/T$, $T = 0.5$ seconds. The form of the surface overpressure given by equations (2-6) through (2-8) has been substituted into equation (2-5) to define the corresponding Rayleigh wave source function for this problem and theoretical time domain fundamental mode Rayleigh wave ground motions have been computed for 3 different ranges using the analytic

18

formulation described in Section 2.2 above. The exact same problem has also been run using a two-dimensional, elastic finite difference code (Auld, 1978) and samples of the results of the two sets of calculations are compared in Figures 2-5 through 2-7. It can be seen that the agreement between the two solutions is excellent at all three distances for times later than the predicted Rayleigh wave arrival times. More surprising at these relatively near-field distances is the fact that for this low frequency loading function almost the entire time history of motion as given by the finite difference solution can be explained in terms of the fundamental mode Rayleigh wave alone.

For purposes of simulating the airblast loading from surface explosions an impulsive approximation to the expanding shock front is required. In the two-dimensional finite difference simulations the airblast was defined by scaling the standard Air Force Weapons Laboratory 1 kt nuclear airblast approximation to 100 tons (Auld et al., 1978). However, since this airblast approximation is not given as an analytic function of time and distance, it is not well suited for incorporation into the analytical Rayleigh wave formulation. Consequently, in the present analysis, the overpressure has been approximated by a series of functions of the form

$$P_m(r,t) = C_m e^{-\alpha_m r} e^{-\beta_m(t - \tau_m)} H(t - \tau_m) \qquad (2-9)$$

where the subscript m denotes the fact that a series of such functions are used to describe the overpressure in various distance ranges and τ_m denotes the arrival time of the airblast at radius r. One of the limitations of this functional form is that it does not model the negative phase which follows the passage of the principal shock. However, over the range of interest here, the contribution of this phase to the total impulse delivered to the ground is relatively small and is not expected to have a

19
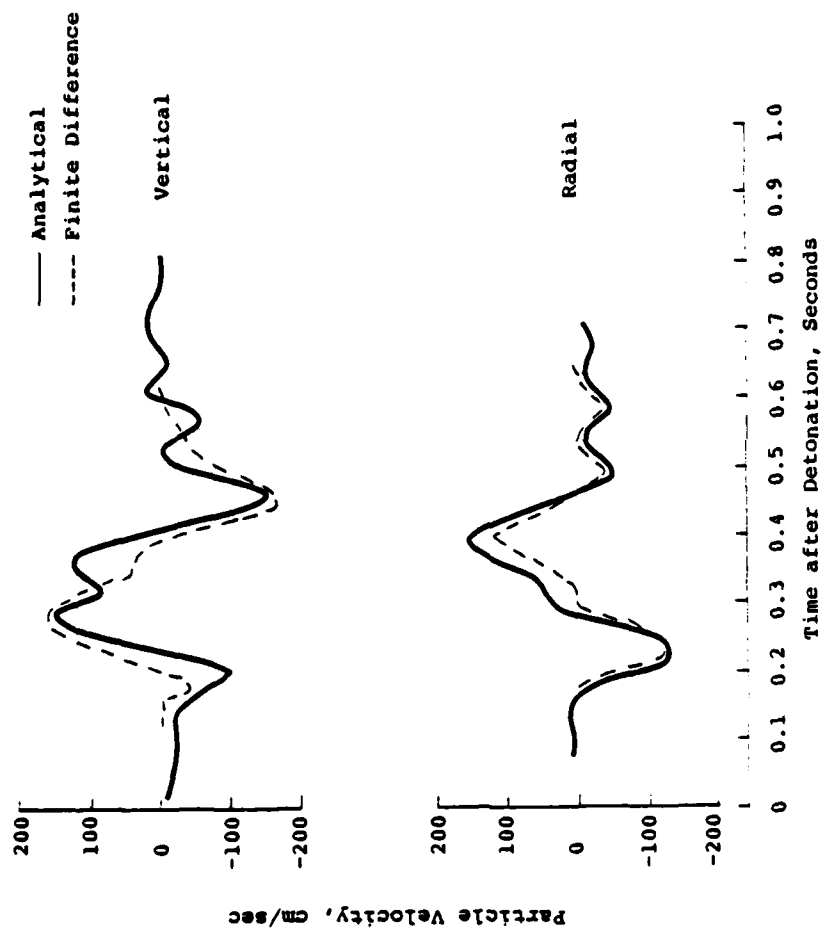
Figure 2-5: Rayleigh Wave Surface Velocity, Pre-Mine Throw Event, r = 85 m. Perfectly Elastic, Overpressure Time Dependence of One-Half Cycle of a 2.0 Hz Sine Wave
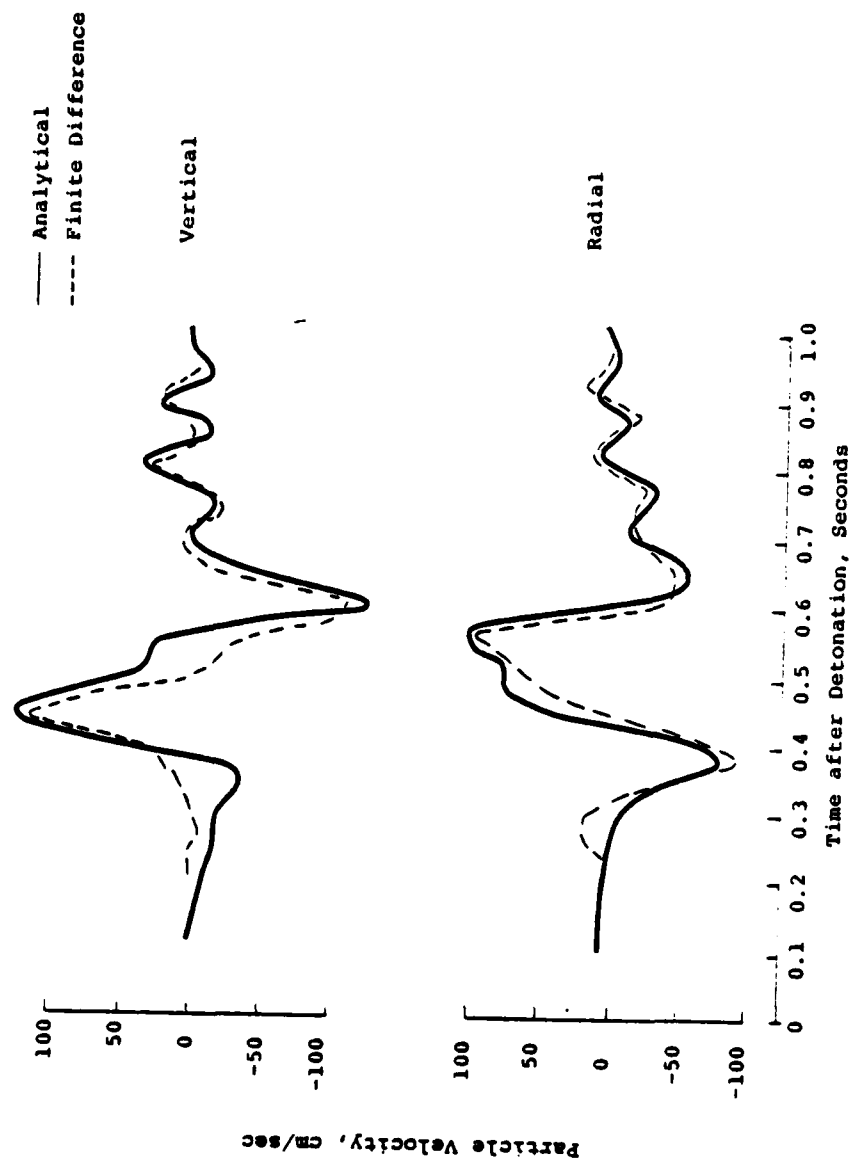
Figure 2-6: Rayleigh Wave Surface Velocity, Pre-Mine Throw Event, r = 150 m. Perfectly Elastic, Overpressure Time Dependence of One-Half Cycle of a 2.0 Hz Sine Wave

21
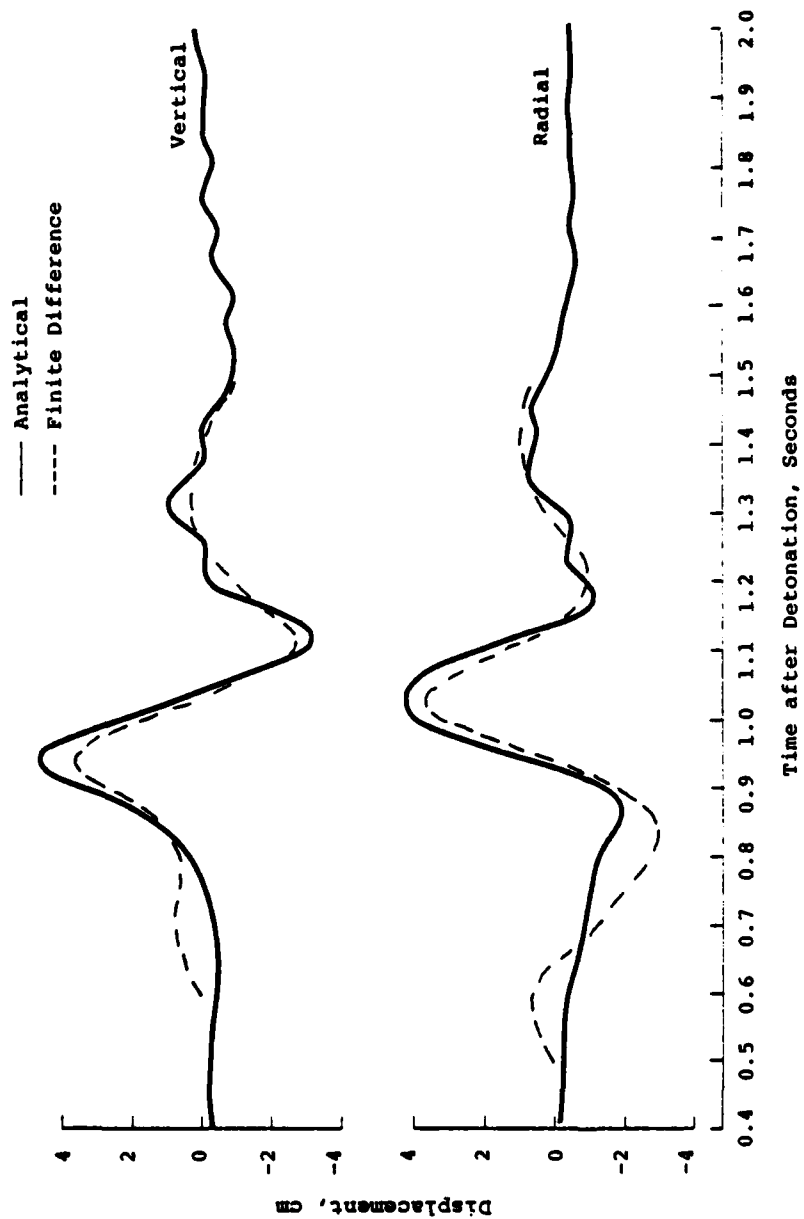
Figure 2-7: Rayleigh Wave Surface Displacement, Pre-Mine Throw Event,
r = 355 m. Perfectly Elastic, Overpressure Time Dependence
of One-Half Cycle of a 2.0 Hz Sine Wave

significant effect on the radiated Raleigh waves. Taking the Fourier transform of equation (2-9) gives

$$p_m(r,\omega) = \frac{C_m e^{-\alpha_m r} e^{-i\omega\tau_m}}{\beta_m + i\omega} \tag{2-10}$$

Then, setting $\tau_m = \tilde{t}_m + r/U_m$ where $\tilde{t}_m$ is the arrival time of the shock at the inner boundary of surface disk m and U_m is the average propagation velocity across disk m, a substitution of equation (2-10) into equation (2-5) gives

$$S_j(\omega) = \sum_{m=1}^{N} \frac{C_m e^{-i\omega\tilde{t}_m}(\beta_m - i\omega)}{\beta_m^2 + \omega^2} \left[\int_{r_{m-1}}^{r_m} r' e^{-\alpha_m r'} J_o(k_j r') \cos\frac{\omega}{U_m} r' \, dr' \right.$$

$$\left. -i \int_{r_{m-1}}^{r_m} r' e^{-\alpha_m r'} J_o(k_j r') \sin\frac{\omega}{U_m} r' \, dr' \right] \tag{2-11}$$

for the Rayleigh wave function for mode j. For both PMT and PDT, the overpressure has been fitted in four concentric surface disks with the parameters indicated in Table 2-1. It can be seen from this table that the innermost disk extending from the origin out to about 11 m is loaded with an overpressure which is much smaller than that which would be predicted by a direct scaling of the 1 kt standard. This reflects the fact that in the corresponding finite difference simulations the actual surface loading begins not at the detonation time but after one time step has elapsed in the calculation. For the time steps employed in the PMT and PDT simulations, the shock front has propagated to a range of about 11 m in the first time step and consequently the disk inside of this radius is loaded only by the low amplitude tail of the pulse as indicated by the parameters in Table 2-1.

Figure 2-8 shows a comparison of the ground motions computed for the loading function (2-9) using both the finite difference and analytical Rayleigh wave procedures. It can be seen that for this impulsive loading condition, the finite difference solution clearly shows the influence of

23

Table 2-1

Parameters for the HE Overpressure Approximation

i	r_{m-1} (m)	r_m (m)	C_m (psi)	α_m (m^{-1})	β_m (sec^{-1})	U_m (m/sec)
1	0	11.4	3,500	0	500	17,980
2	11.4	30.5	33,666	0.045	200	2,865
3	30.5	122	1,124	0.011	80	610
4	122	305	36	0.0024	20	381
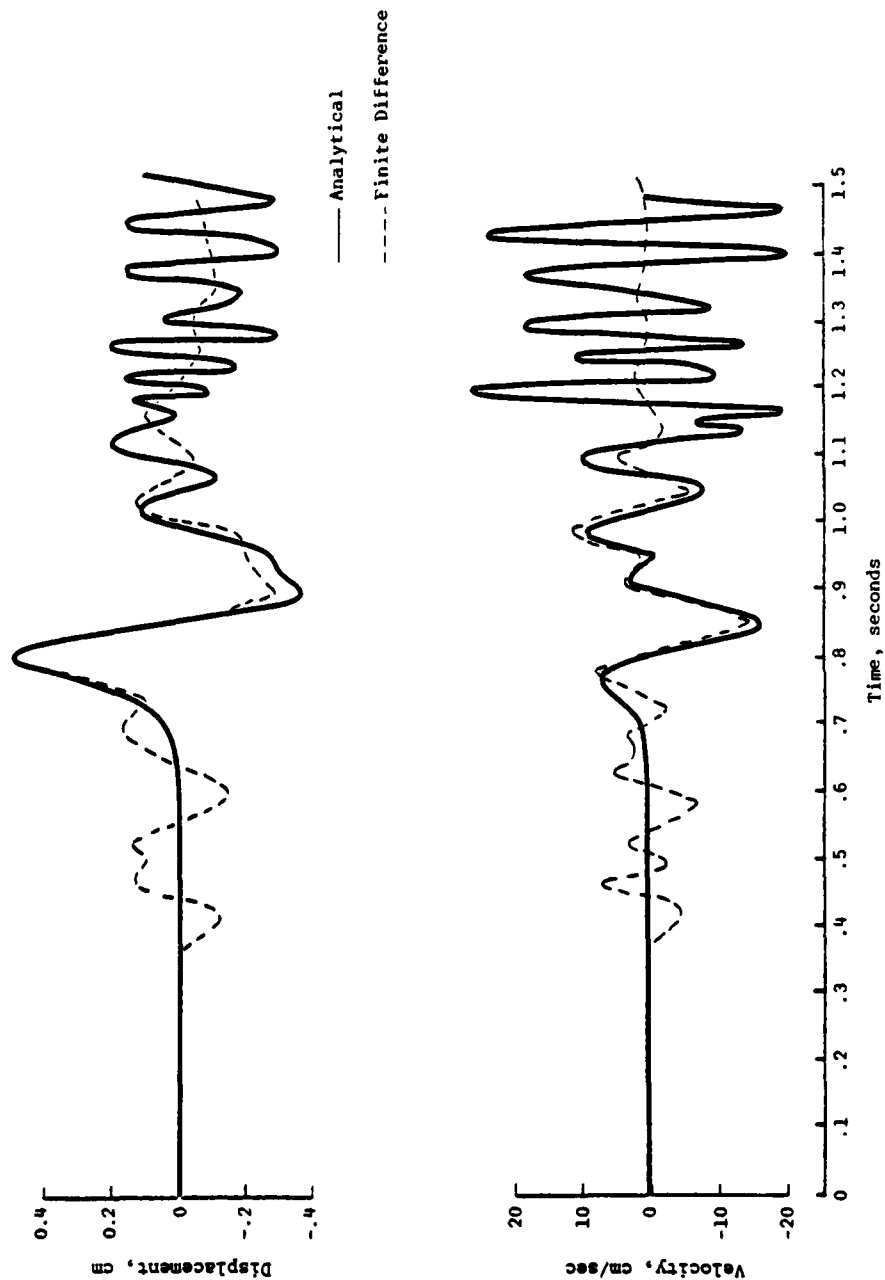
Figure 2-8: Comparison of Finite Difference and Analytical Surface Wave Solutions for Pre-Mine Throw; r = 355 m.

25

body wave arrivals not included in the analytic solution. However, the initial low frequency contributions to the motion which arrive at the expected Rayleigh wave arrival time are again in excellent agreement. It can also be seen that in this case the agreement at late times is not nearly as good as in the case of the low frequency test case described above. This is apparently due to the fact that the late arriving, high frequency components of the surface wave predicted by the analytical model are not reproduced by the finite difference calculation. Similar comparisons at a variety of different distances suggest that this effect is not due to propagation losses through the finite difference mesh. Rather, it appears that the effective loading function "seen" by the finite difference model at high frequencies does not exactly match that implied by equation (2-9). The source of this discrepancy is not known at the present time. One possibility is that the artificial viscosity used to control the discontinuous shock fronts in the finite difference code may be attenuating the high frequency energy coupling to some extent. In any case, it has been found that the two solutions can be brought into excellent agreement if the analytical surface wave motion is modified by passing the signal through a second order lowpass filter with a corner frequency of 2.5 Hz. Consequently, in all the comparisons shown in this section, the analytical Rayleigh wave signals have been processed using this filter.

One of the advantages of the analytic formulation of the problem is that the contributions to the total solution arising from different components of the forcing function can be easily evaluated. This is illustrated in Figure 2-9 which shows the contributions to the fundamental mode Rayleigh wave source function arising from the various surface disks used in modeling the airblast from the Pre-Mine Throw explosion (cf Table 2-1). It can be

26
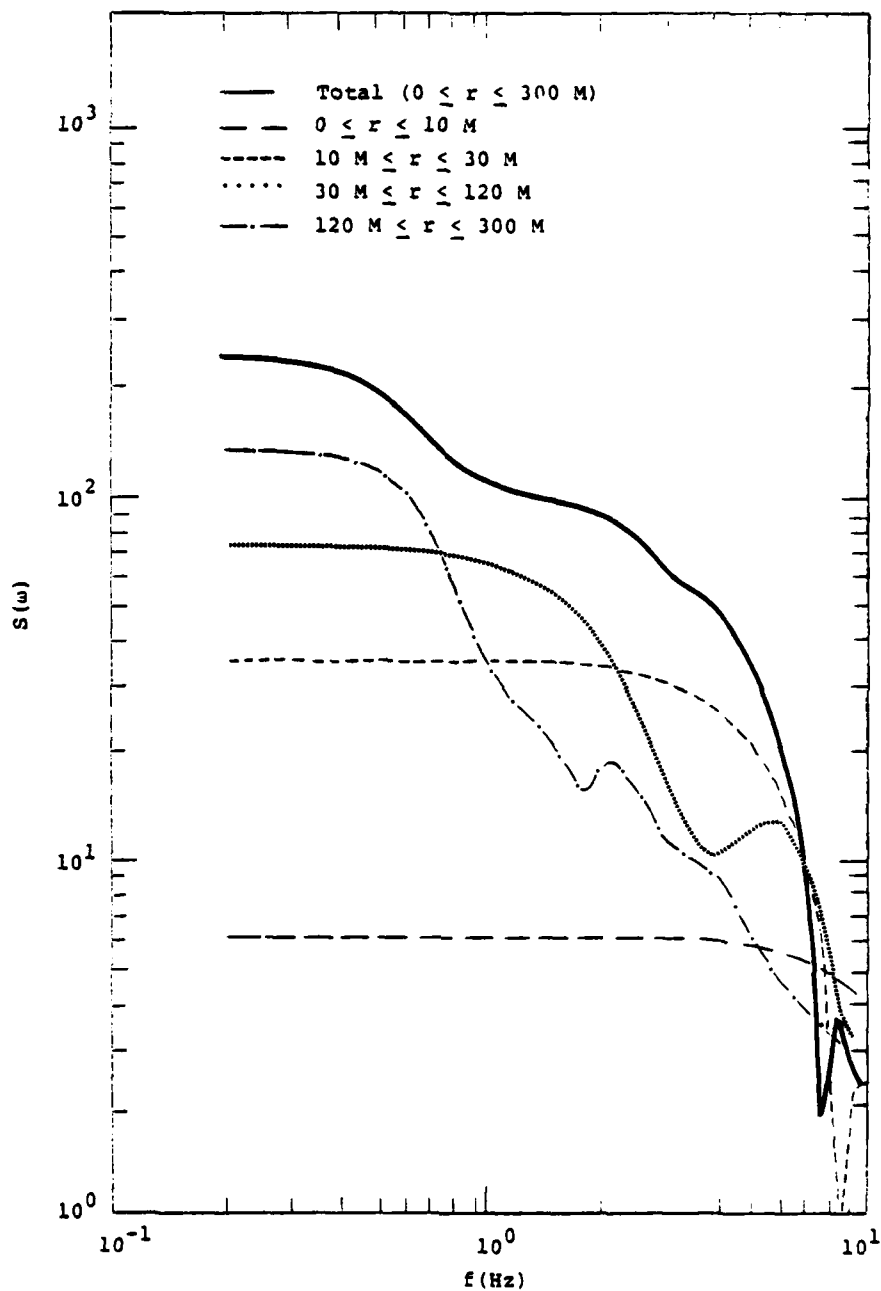
Figure 2-9: Comparison of the Components of the Pre-Mine
Throw Rayleigh Wave Source Function due to
Airblast Loading of Various Surface Disks

27

seen that over the frequency range of interest in this application (i.e. about 2 to 8 Hz) the fundamental mode Rayleigh waves are generated primarily by the airblast loading extending from about 10 to 120 m from ground zero. Figure 2-10 shows the theoretical, vertical component, fundamental mode Rayleigh wave displacement spectrum for Pre-Mine Throw (i.e. the modulus of $W_j(r, \omega)$ given by equation (2-4) multiplied by the modulus of the second-order lowpass filter). This figure indicates that the vertical component Rayleigh wave displacement time histories can be expected to be dominated by frequency components in the 2.0 to 3.0 Hz range.

The ground motions computed for an airblast load acting on the surface of the PMT geologic model using both the finite difference code and the analytical fundamental mode Rayleigh wave solution are compared at three different ranges in Figures 2-11 through 2-13 for the time intervals following the theoretical arrival times of the Rayleigh waves. It can be seen from these figures that the two solutions are generally in excellent agreement over the time interval of interest. At the two closer stations (i.e. 83 m and 152 m) there are some discrepancies at early times which indicate interference between body wave and surface wave arrivals in the finite difference solution. Moreover, the solutions for the vertical displacements at these two stations show a nearly constant offset which appears to be related to the directly induced effects of the late-time overpressure which are not included in the analytical solution. In any case, the comparisons provide strong evidence that the late-time, low frequency components of motion on the finite difference simulation of PMT are fundamental mode Rayleigh waves.

It was noted previously that the finite difference ground motion simulation of the PMT experiment agreed well with the data measured from

28
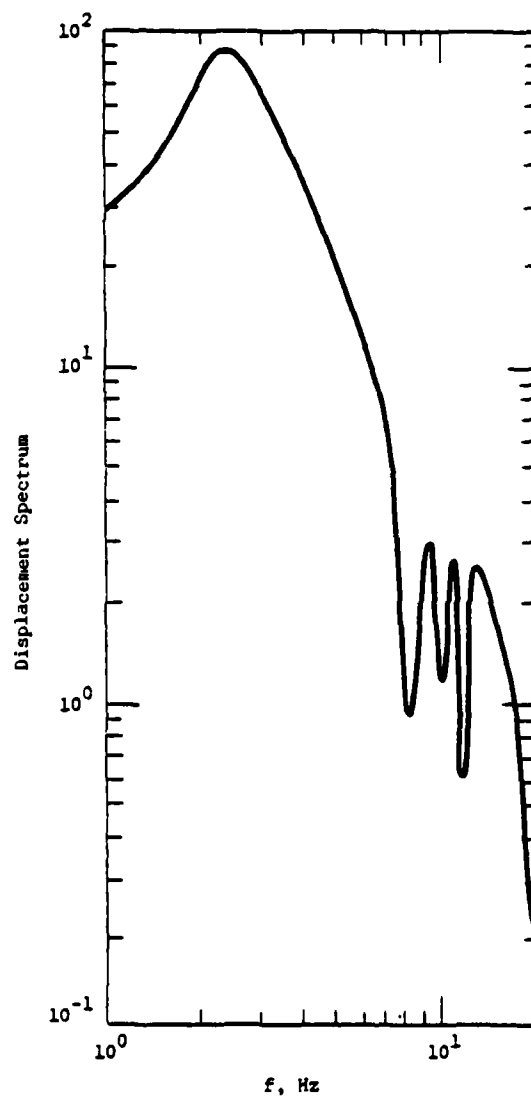
Figure 2-10:   Theoretical, Vertical Component,
              Fundamental Mode Rayleigh Wave
              Displacement Spectrum for Pre-
              Mine Throw
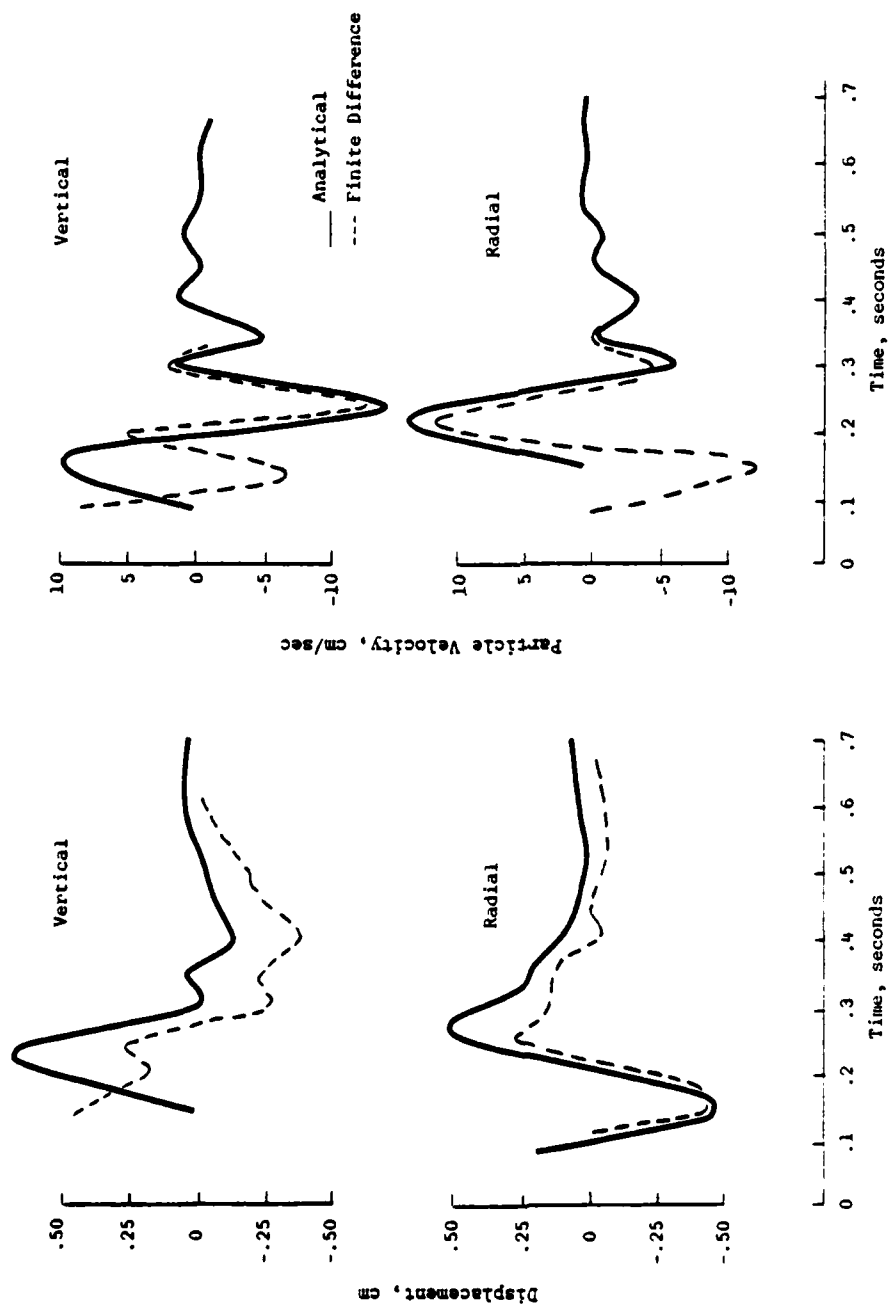
Figure 2-11: Comparison of Finite Difference and Analytical Surface Wave Solutions for Pre-Mine Throw, r = 83 m.
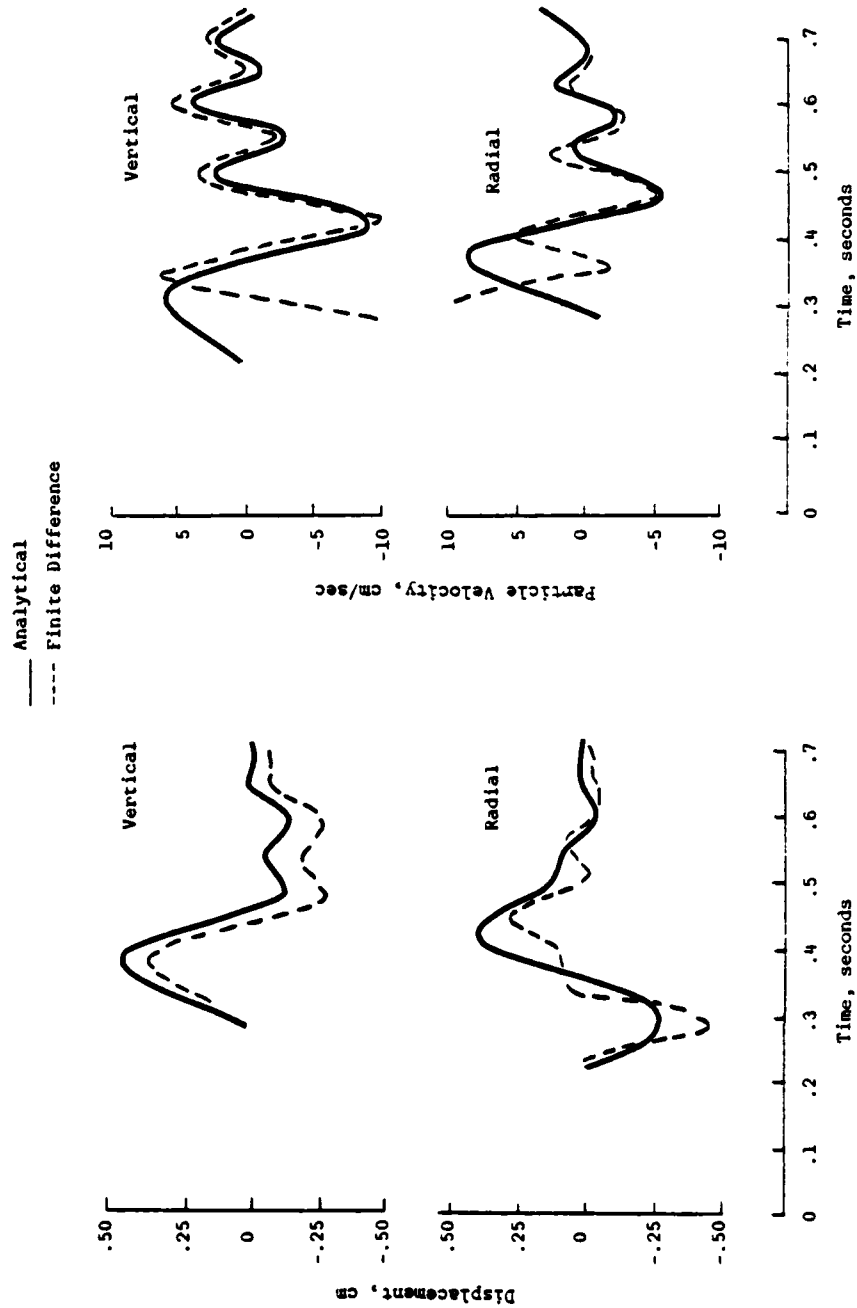
Figure 2-12: Comparison of Finite Difference and Analytical Surface Wave Solution for Pre-Mine Throw, r = 152 m.

31
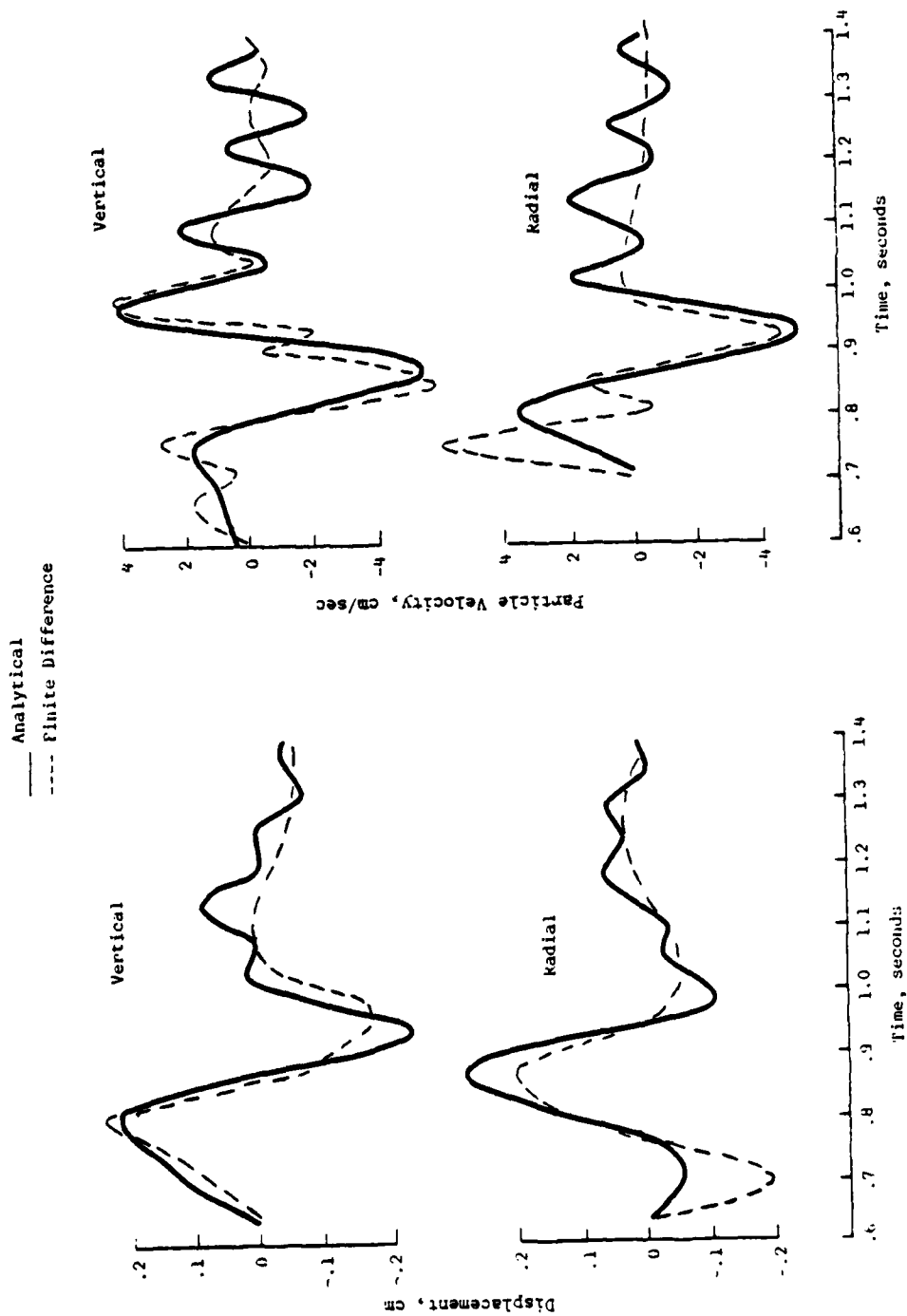
Figure 2-13: Comparison of Finite and Analytical Surface Wave Solutions for Pre-Mine Throw, r = 355 m.

this event (Auld et al., 1978). Thus, given the comparisons shown in Figures

2-11 through 2-13, it can be anticipated that the analytical Rayleigh wave

solution agrees well with the late-time portions of the observed ground

motion. This is found to be the case as is shown in Figures 2-14 through

2-17 which show comparisons with the available data. Figure 2-14 shows

comparisons with data measured at the same distance along two different

azimuths which demonstrate the consistency of the data measured from this

event. It should be noted that the "observed" displacements on these figures

were derived from the measured velocities and, consequently, are of questionable

reliability due to the uncertainties in the baseline corrections. In any

case, with the exception of some small discrepancies in arrival time which

are probably related to lateral heterogeneities in the subsurface geology,

the agreement between the observed data and the calculated airblast induced

fundamental mode Rayleigh wave is remarkably good with respect to both

amplitude level and wave shape. Thus, most of the observed surface wave

motion from this event can be accounted for by considering only the airblast-

induced Rayleigh wave motion originating at ranges greater than 11 m from

ground zero. The conjecture is that the loading inside of this radius is

not efficiently coupled into radiated surface waves due to energy losses

associated with crater formation and other nonlinear interactions which are

known to take place in the immediate vicinity of ground zero. This is a

plausible explanation in this case since the measured crater radius for

PMT was about 10m.

2.3.3 Pre-Dice Throw Rayleigh Wave Simulation

An analysis similar to that described above for PMT has also been

performed for the PDT experiment. Figure 2-18 shows the contributions to

the fundamental mode Rayleigh wave source function arising from the various

33
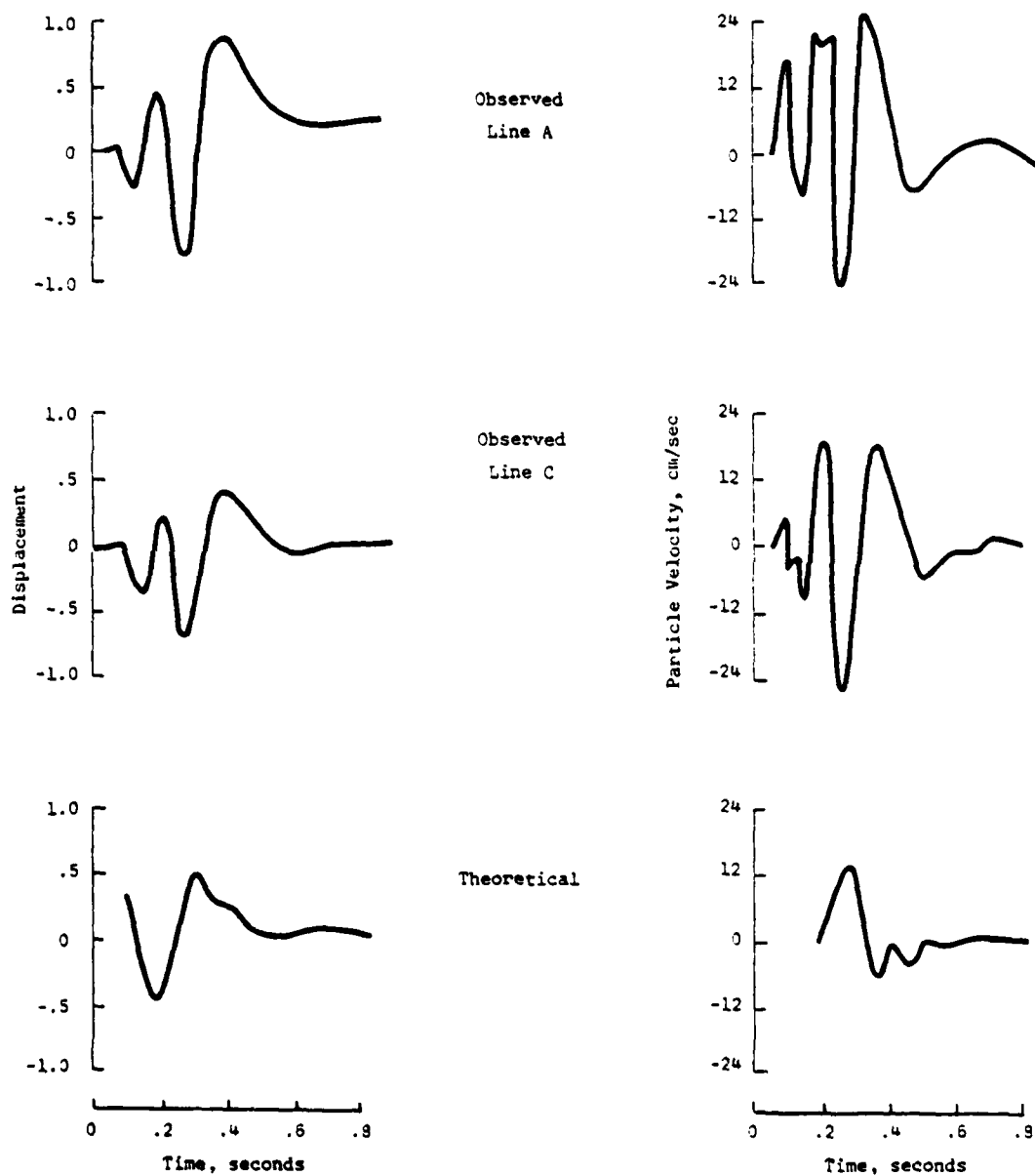
Figure 2-14: Comparison of Observed and Calculated Rayleigh Wave Motion, Pre-Mine Throw, Radial Component, r = 83 m.
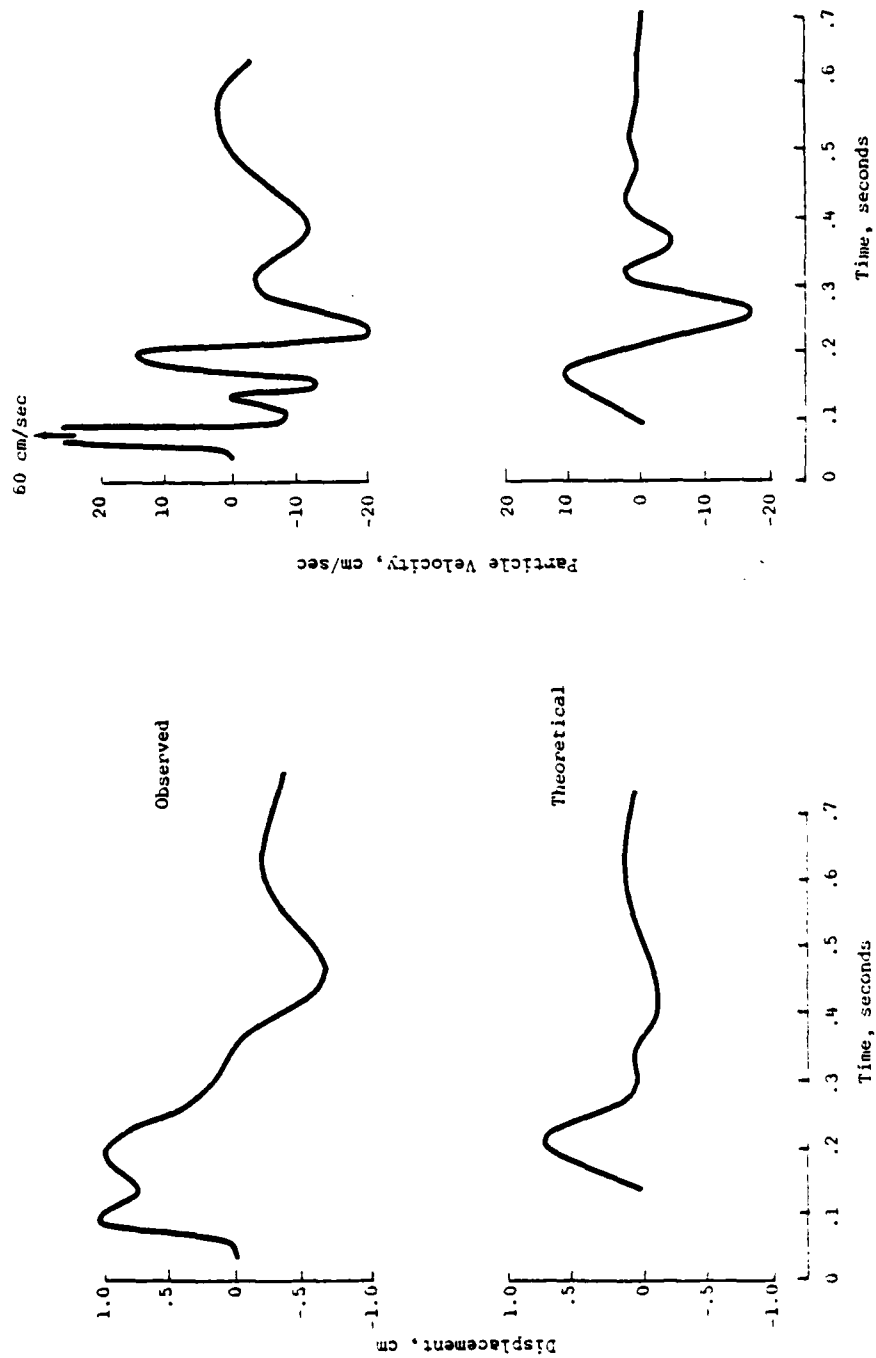
Figure 2-15: Comparison of Observed and Calculated Rayleigh Wave Motion, Pre-Mine Throw, Vertical Component, r = 83 m.

35
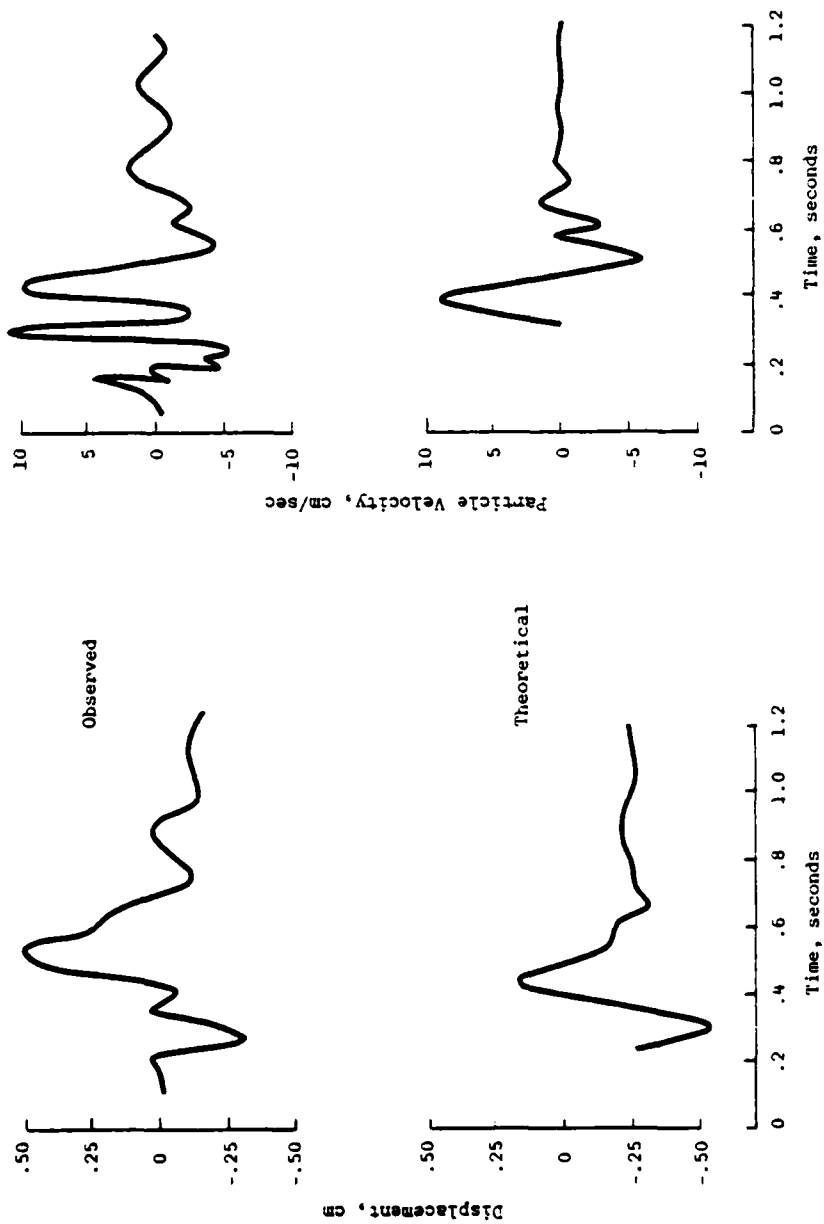
Figure 2-16: Comparison of Observed and Calculated Rayleigh Wave Motion, Pre-Mine Throw, Radial Component, r = 152 m.
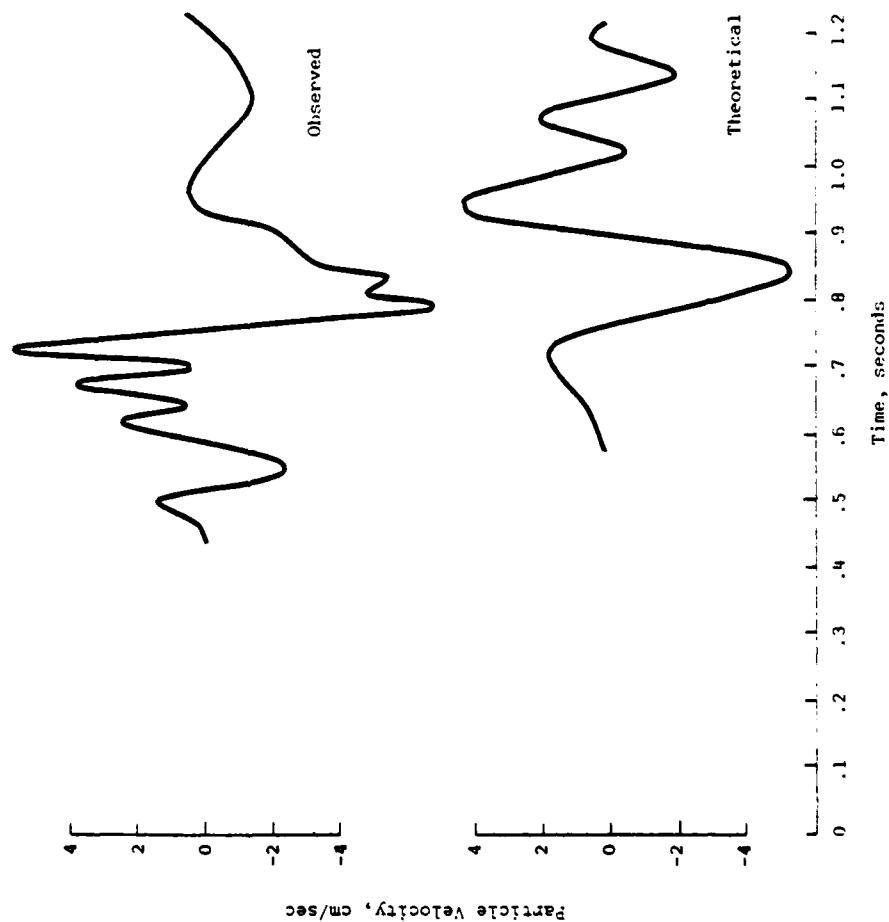
Figure 2-17: Comparison of Observed and Calculated Rayleigh Wave Motion, Pre-Mine Throw, Vertical Component, r = 355 m.

37
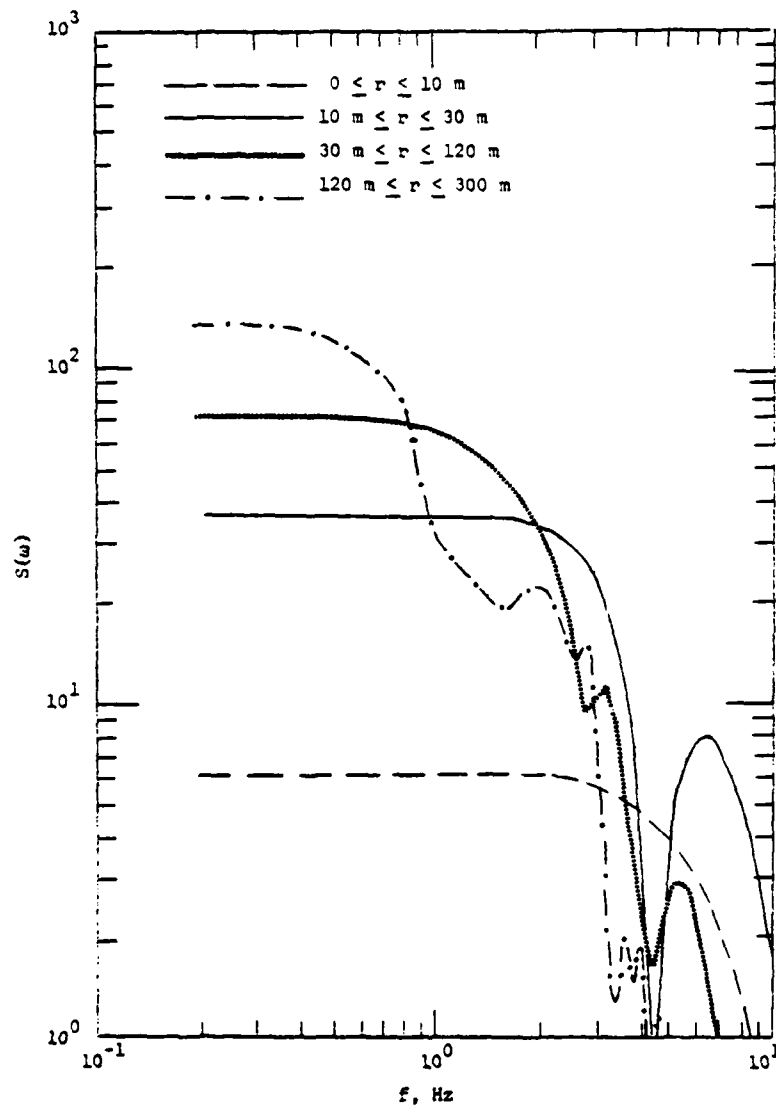
Figure 2-18: Comparison of the Components of the
Pre-Dice Throw Rayleigh Wave Source
Function due to Airblast Loading of
Various Surface Disks

38

surface disks used in modeling the airblast from PDT. It can be seen that as

for PMT, over the frequency range of interest (i.e. about 2 to 4 Hz), the

fundamental mode Rayleigh wave excitation is dominated by the airblast loading

extending from about 10 to 120 m from ground zero. A comparison with Figure

2-9 indicates that the PDT source function falls off sharply above about 3.0 Hz

as opposed to the PMT source function which is flat out to about 5.0 Hz. This

effect is related to the fact that the Rayleigh wave propagation velocities for

PDT are significantly lower than those for PMT. The theoretical, vertical-

component, fundamental-mode Rayleigh wave displacement spectrum for PDT is

shown in Figure 2-19. As with PMT, comparisons have indicated that the finite

difference and analytical solutions can be brought into agreement if the analy-

tical surface wave motion is lowpass filtered, in this case using a second order

filter with a corner frequency of 1.5 Hz. Consequently, the effect of this

filter has been included in the spectrum shown in Figure 2-19 and in all the

time history comparisons shown in this section. A comparison of Figure 2-19 with

the corresponding PMT spectrum shown previously in Figure 2-10 indicates that

the theoretical PDT Rayleigh wave signal is very narrowband with respect to

the PMT Rayleigh wave signal and would be expected to be dominated by components

with frequencies in the 2.0 to 3.0 Hz range.

The ground motions computed for an airblast load acting on the surface

of the PDT geologic model using both the finite difference code and the

analytical Rayleigh wave solution are compared at three different ranges in

Figures 2-20 through 2-22 for the time intervals following the theoretical

arrival times of the fundamental mode Rayleigh waves. As with PMT it can be

seen that the two solutions are generally in excellent agreement over the time

interval of interest, particularly for the ranges of 90 and 180 m. At the most
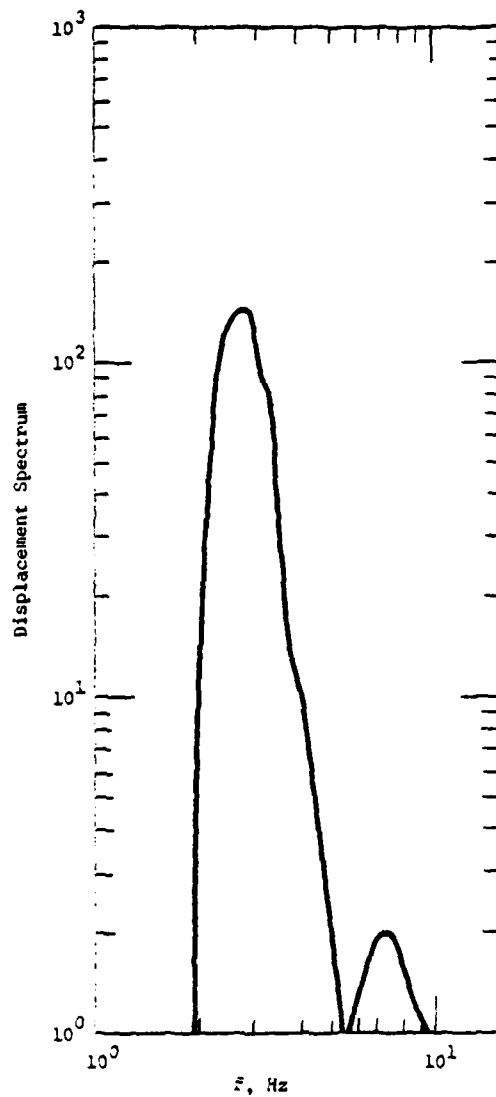
Figure 2-19: Theoretical, Vertical Component, Fundamental Mode Rayleigh Wave Displacement Spectrum for Pre-Dice Throw

40
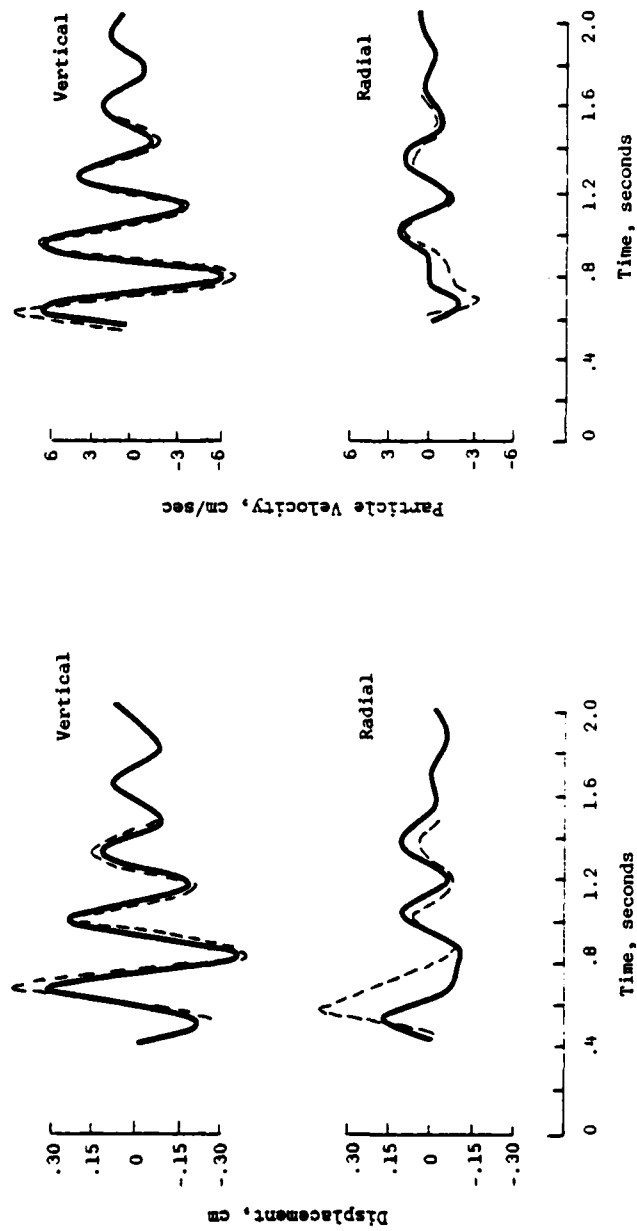
Figure 2-20: Comparison of Finite Difference and Analytical Surface Wave Solutions for Pre-Dice Throw, r = 90 m.

41
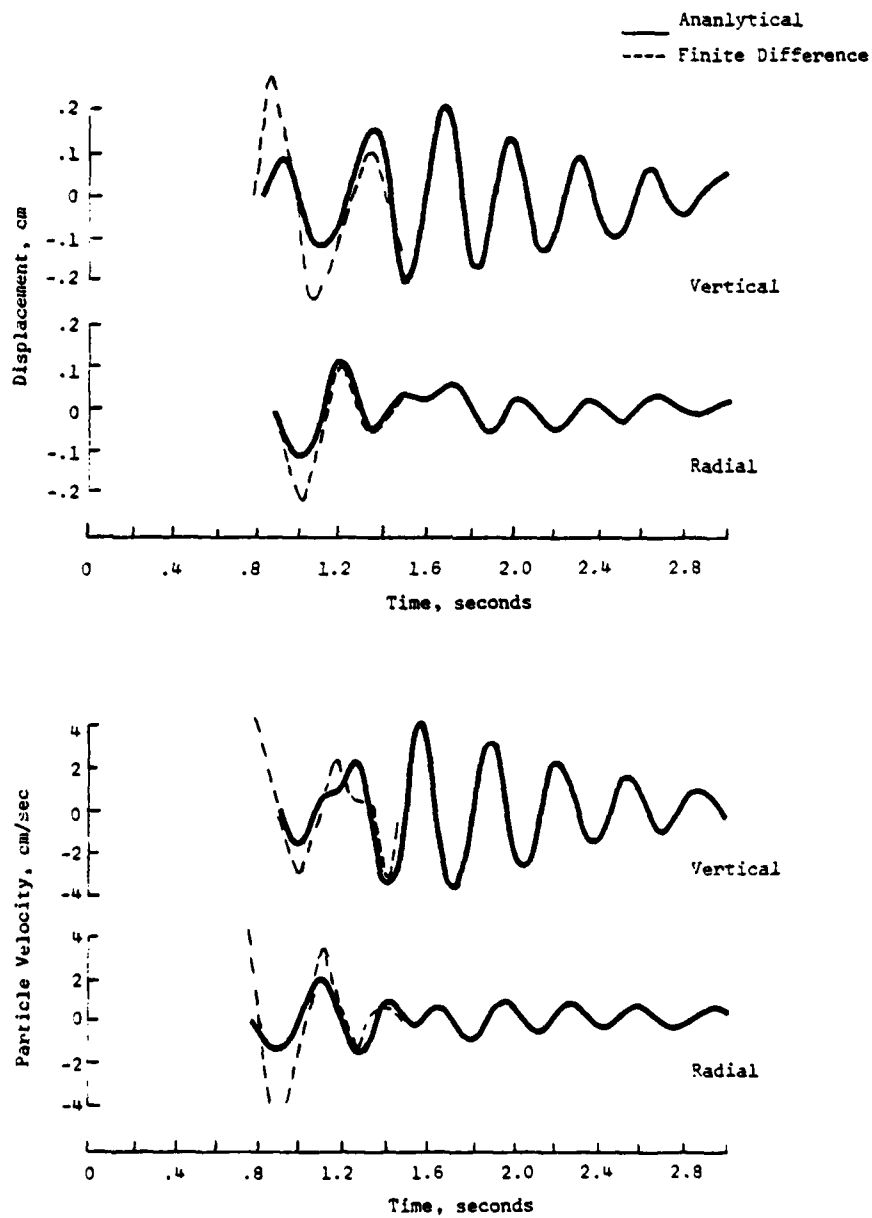
Figure 2-21: Comparison of Finite Difference and
Analytical Surface Wave Solutions for
Pre-Dice Throw, r = 180 m.

42
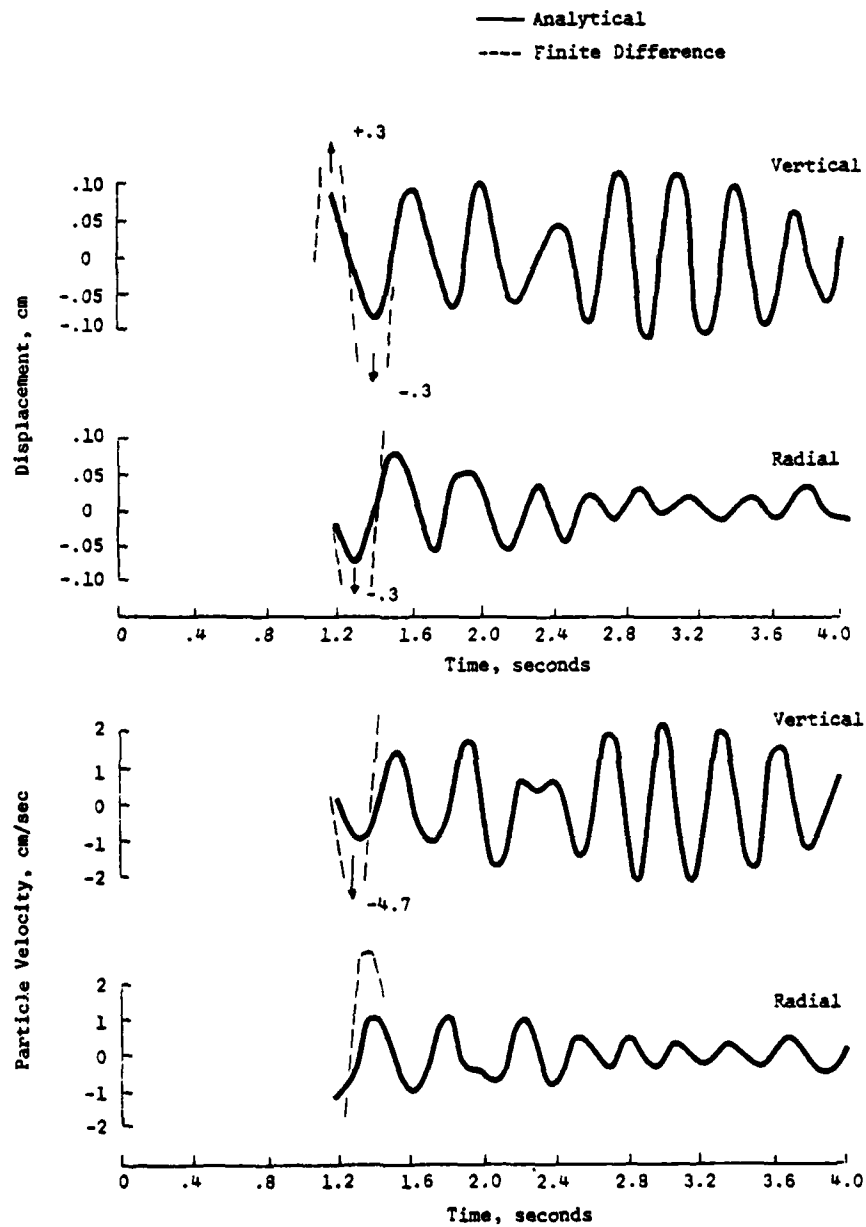
Figure 2-22: Comparison of Finite Difference and Analytical Surface Wave Solutions for Pre-Dice Throw, r = 310 m.

43

distant range (i.e. 310 m), the amplitude of the analytical solution is
considerably lower than that of the finite difference solution, although it is
difficult to assess the significance of this discrepancy since there is only
about one cycle of motion to compare at this range due to the termination of
the finite difference calculation at 1.5 seconds after detonation time. It
can be seen that in this case the time histories are very nearly sinusoidal
and are of long duration relative to those computed at similar distances for
PMT, as would be expected from the differences in the spectra noted above.
It is also interesting to note from these figures that the unusually small
ratio of radial to vertical component surface wave amplitude level (i.e.
ellipticity) predicted theoretically for the PDT geologic model is substantiated
by the finite difference calculations.

In the process of making the comparisons shown in Figures 2-20 through
2-22, it was noted that the low frequency motion on the finite difference
solutions consistently appeared to arrive before the time predicted for the
fundamental mode Rayleigh wave. This suggested the possibility that higher
modes might be contributing in this case, and further investigation indicated
that these earlier arrivals could in fact be explained by adding the contri-
bution due to the first higher Rayleigh mode. Figure 2-23 shows comparisons
of the Rayleigh wave dispersion and site response curves for the fundamental
and first higher mode at the PDT site. It can be seen that the first higher
mode is associated with higher propagation velocities and a shift in the site
response to higher frequencies relative to the fundamental mode. Investigation
of the characteristics of still higher modes indicates that they are not expected
to contribute significantly over the frequency range of interest here. However,
since the addition of the contribution from the first higher mode does improve
the comparisons with the finite difference calculations, it has been included

44
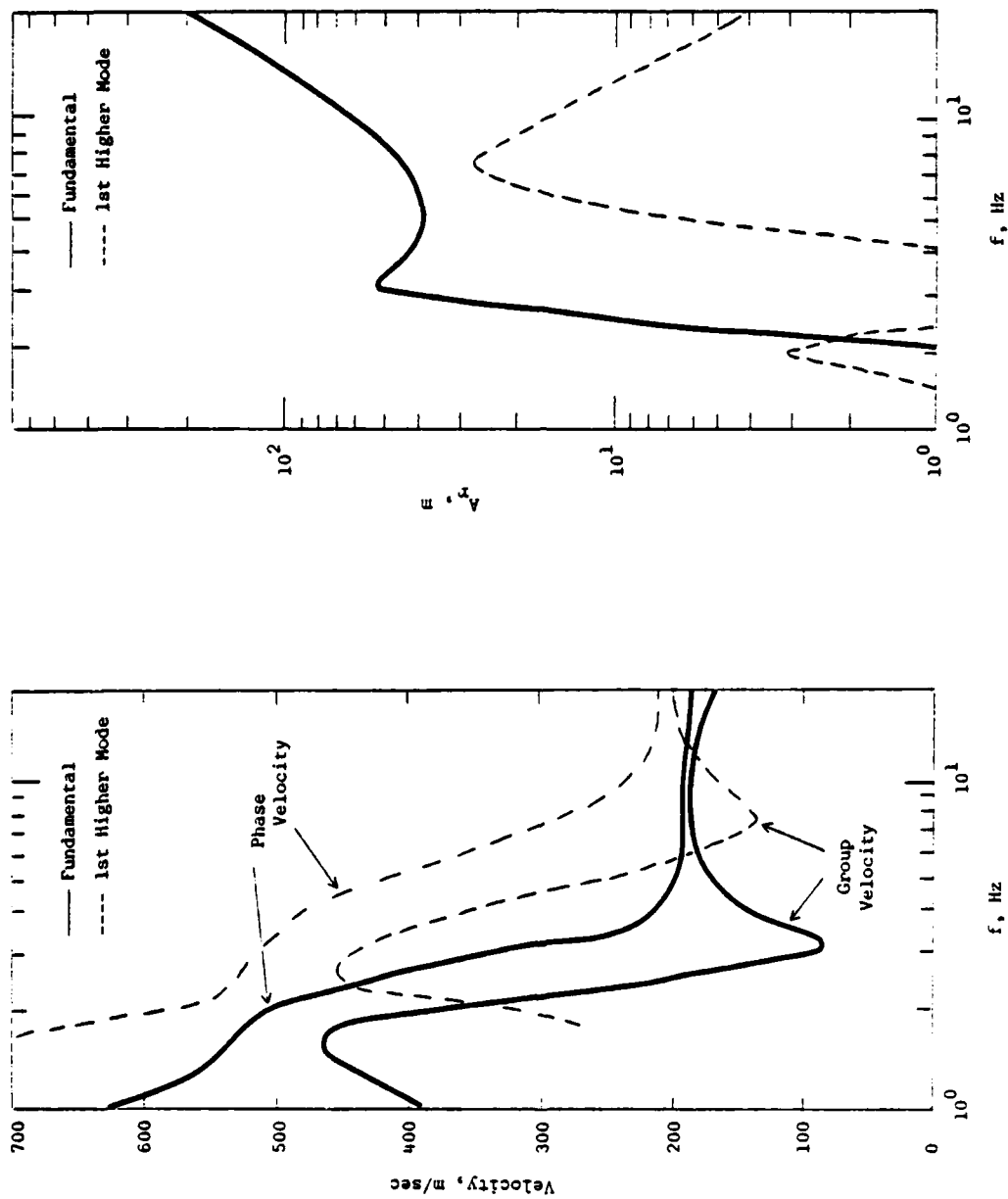
Figure 2-23: Comparison of Rayleigh Wave Dispersion and Site
Response Curves for the Fundamental and First
Higher Mode, Pre-Dice Throw Site

in the synthesis of the Rayleigh wave motion used in the comparison with the observed data.

Figures 2-24 through 2-27 show comparisons of the calculated Rayleigh wave ground motions with the observed data from PDT. It can be seen that in this case the agreement between the computed and observed waveforms is not as remarkable as it was for PMT. However, the general frequency content and amplitude level of the observed data are again reproduced quite faithfully by the theoretical elastic calculation. Thus, as in the case of PMT, it appears that most of the observed surface wave motion for PDT can be accounted for by considering only the airblast induced Rayleigh wave motion originating at ranges greater than about 11 m from ground zero. The physical significance of the 11 m radius is not clear in this case, however, since the measured crater radius for PDT was greater than 20 m. Thus, it is clear that significant nonlinear interactions were occurring at least to this range for PDT. It has not yet been determined how much the agreement between the computed and observed surface wave motion would be affected by applying a reduced airblast load over a surface disk extending to 20 m rather than the current 11 m.

2.4 Conclusions

The analyses described in this chapter have centered on the evaluation of the low frequency, oscillatory components of motion which are typically observed on the ground motion records from surface explosions. This motion has been conclusively identified as a classical Rayleigh-type surface wave using the theoretical solution of the problem for surface waves generated in a multilayered, elastic halfspace by an axisymmetric airblast load. This analytical model has been used to simulate the Rayleigh waves for the PMT and PDT experiments, and it has been found that the observed surface wave data from these events can be matched surprisingly well by considering only the airblast induced elastic motions originating at ranges greater than about 11 m

46
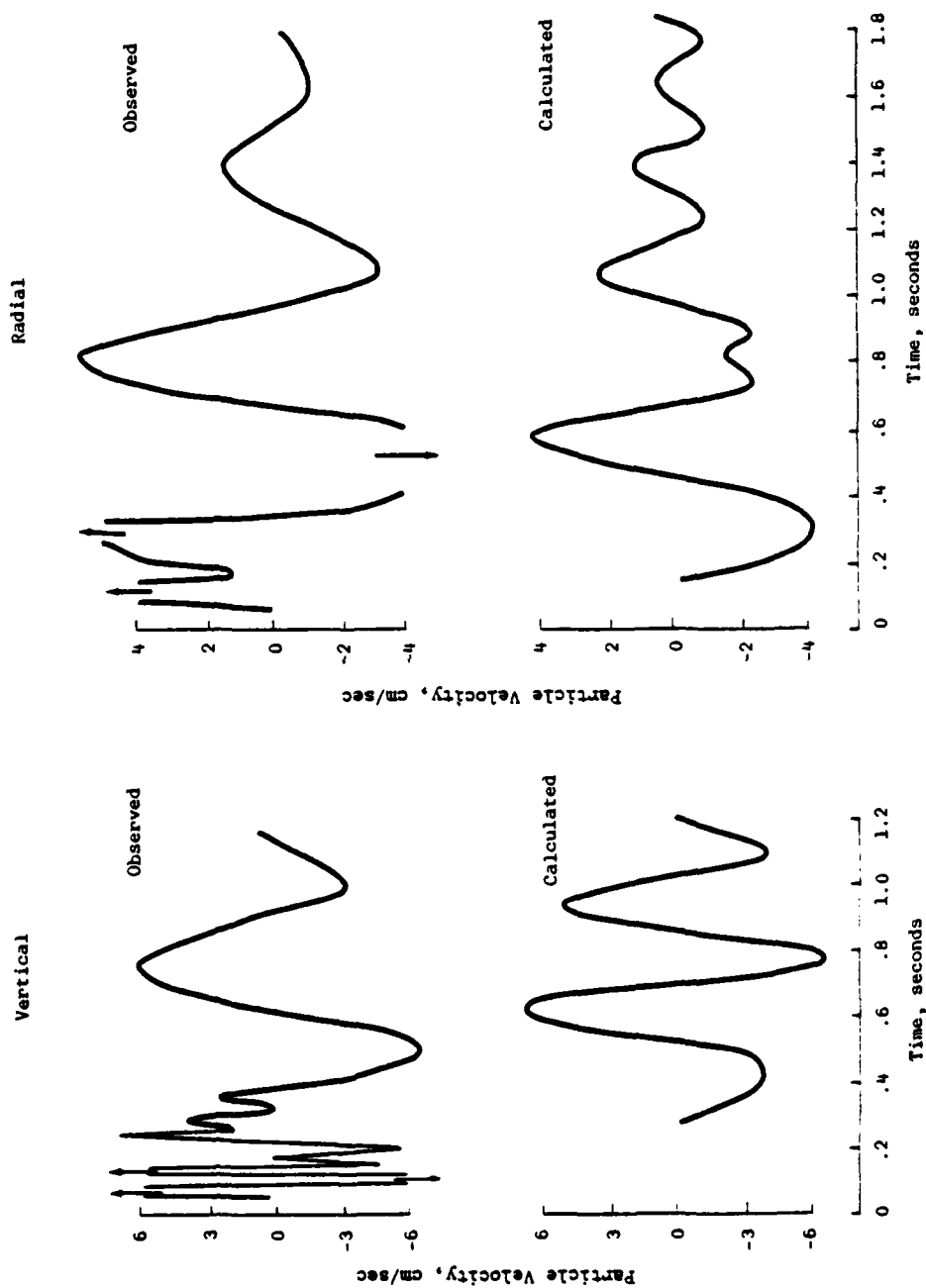
Figure 2-24: Comparison of Observed and Calculated Rayleigh Wave Motion, Pre-Dice Throw, r = 90 m.

47
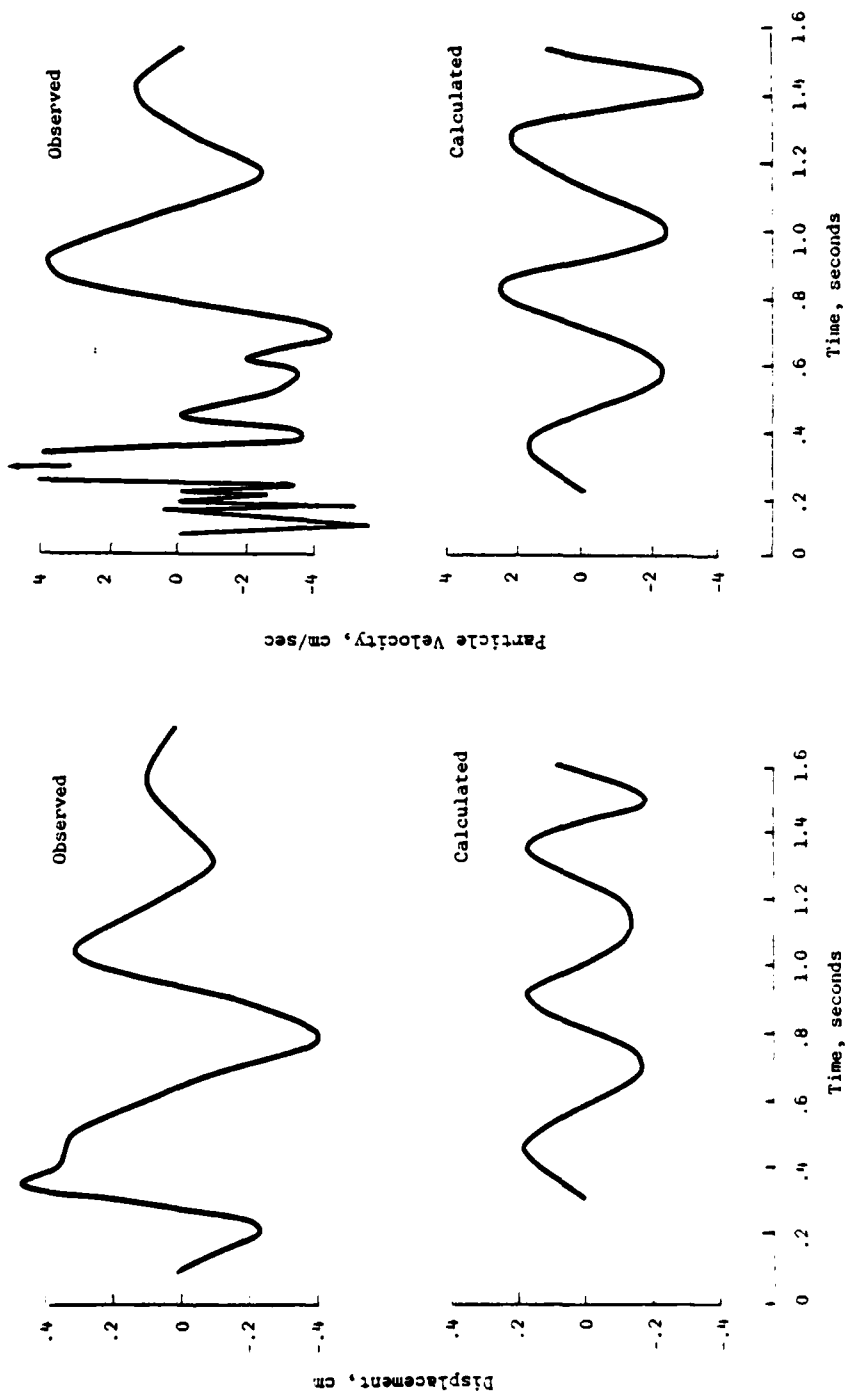
Figure 2-25: Comparison of Observed and Calculated Rayleigh Wave Motion, Pre-Dice Throw, Vertical Component, r = 180 m.
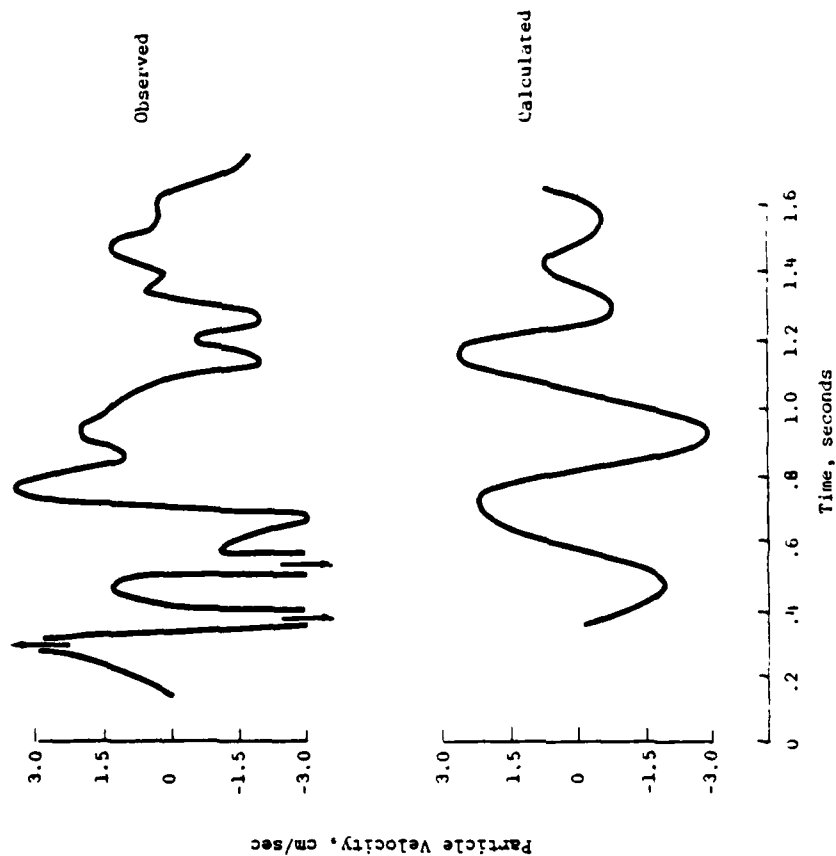
Figure 2-26: Comparison of Observed and Calculated Rayleigh Wave Motion, Pre-Dice Throw, Radial Component, r = 180 m.
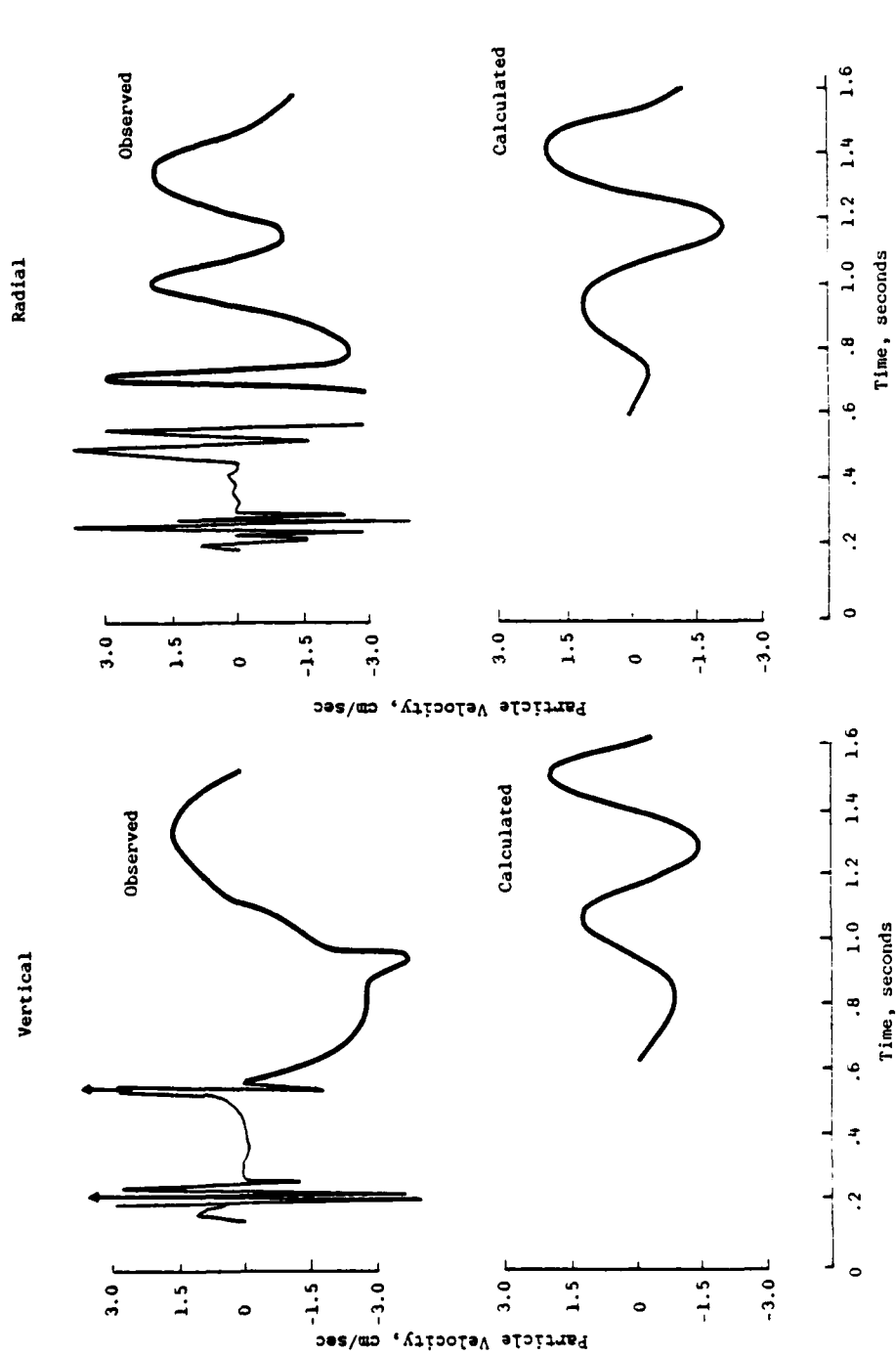
Figure 2-27: Comparison of Observed and Calculated Rayleigh Wave Motion, Pre-Dice Throw, r = 310 m.

50

from ground zero. The inference albeit conjectural is that the loading inside of this radius is not efficiently coupled into radiated surface waves due to energy losses associated with crater formation and other nonlinear inter-actions which are known to take place in the vicinity of ground zero. This suggests that it may be possible to estimate significant portions of the radiated elastic wave field from such explosions using simple approximations to the seismic source function.

Chapter 3

Valley Reverberation Studies

3.1 Introduction

Many of the deployment options currently being considered for the MX system involve sites located in one or more of the large alluvial valleys typical of the Basin and Range geologic province which covers much of the Southwestern U.S. Thus, one of the questions relating to the definition of the ground motion environment concerns the extent to which the presence of the valley boundaries will influence the late-time motions to be expected at sites within the valley. The analyses described in this section have focused on an attempt to assess the magnitude of this effect using ground motion data recorded from underground nuclear tests conducted at the NTS. Two sets of ground motion data have been studied. The first is composed of data recorded on a dense array of seismometers located in the Las Vegas Valley at a range of about 150 km from the source area on NTS and is well suited for detailed analyses of reflected arrivals originating at the valley boundaries. The second set includes data recorded on the edge of Yucca Valley at ranges of less than 10 km. While these latter data were not recorded on the type of instrumentation arrays which are well suited for studying the details of the interactions with the valley boundary, they complement the Las Vegas data by providing a general picture of the phenomenon at distance ranges which are more directly relevant to MX deployment.

3.2 Analysis of the Las Vegas Valley Data

The Las Vegas Valley is a prominent northwest trending topographic depression situated in the southern part of the Basin and Range Province. The city of Las Vegas is located in the southern portion of this elongated valley

52

in the center of a rectangular basin which is about 30 km wide and 40 km long. The city has been well instrumented to record ground motions from underground nuclear tests conducted at NTS, which is located about 150km to the northwest of Las Vegas. Figure 3-1 shows the locations of a selected subset of these stations and Figure 3-2 shows the radial component velocity time histories recorded at these stations from the CARPETBAG explosion. These records are typical and show pronounced evidence of interference at late arrival times consistent with what would be expected from the simultaneous arrival of energy from several different directions (Murphy and Hewlett, 1975). Another qualitative measure of the effects of the valley boundaries is provided in Figure 3-3 which shows a comparison of the radial component seismograms recorded in Las Vegas (SE-6) and Pahrump (PAH) from the same explosion. It can be seen that the upper trace, recorded within the Las Vegas Valley, is much more complex and of significantly longer duration than the lower trace which was recorded outside the valley at about the same epicentral distance. The inference is that multipathing of energy along the valley boundaries is the source of this dramatic increase in complexity and duration.

In order to determine the direction of approach and relative amplitude of these secondary arrivals, the data of Figure 3-2 have been velocity filtered using the beam-steer process which is routinely used in the detection and analysis of signals recorded at large seismic arrays such as the Montana LASA. The concept underlying this process is quite simple. Suppose an arrival of interest (e.g., a P wave) is traveling across the array from some unknown direction with phase velocity C. Now for each possible direction of approach, ϕ, there will be a unique set of delays, $\Delta t_i(\phi)$ describing the propagation across the station locations at velocity C. Thus, if the waveforms recorded at each station are time-shifted by an amount $\Delta t_i(\phi)$ and added together, then energy arriving from direction ϕ with velocity C will

53

Figure 3-1: Station Location Map for Las Vegas
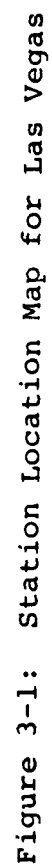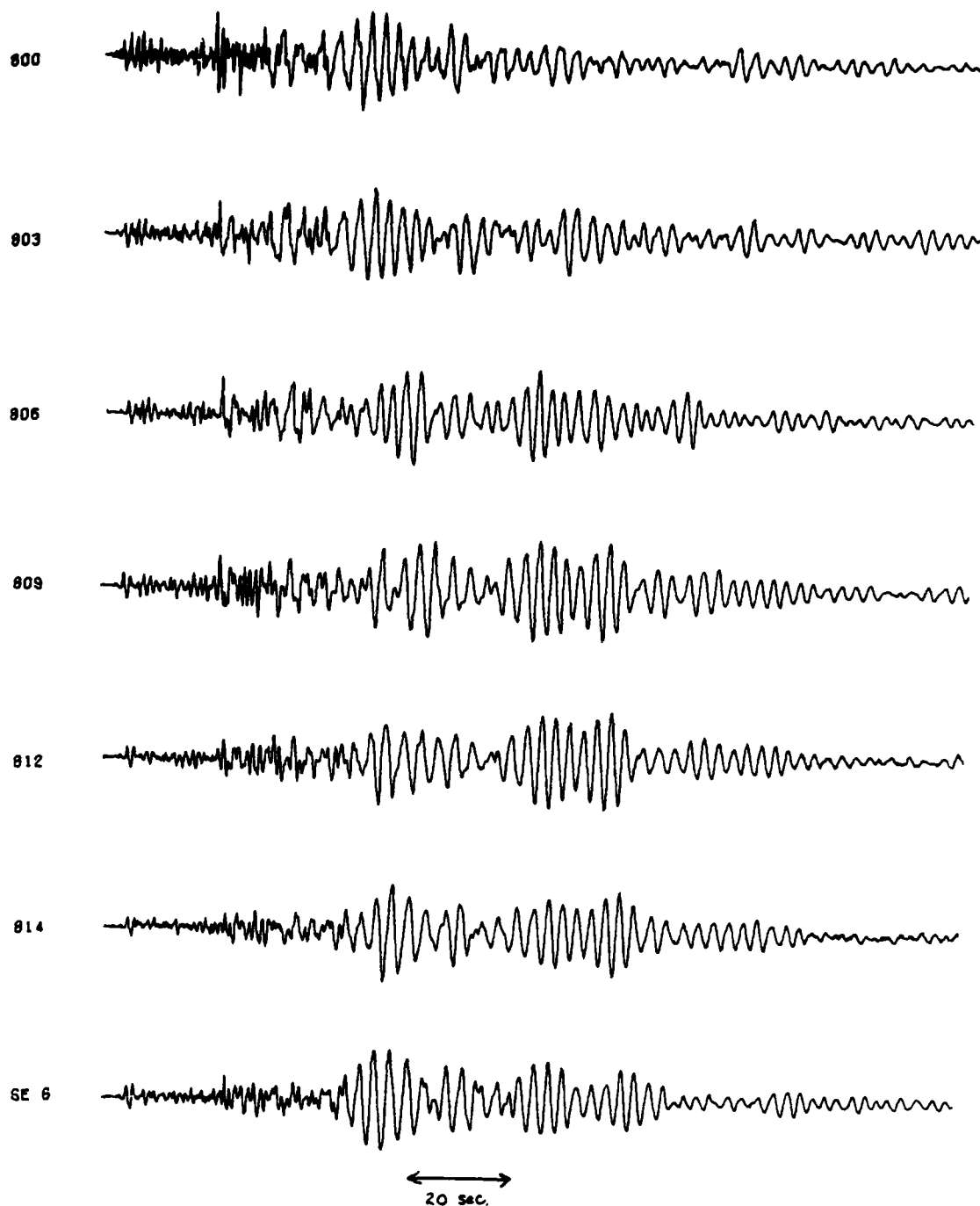
Figure 3-2:   Radial Component Record Section
for the Carpetbag Event

FONTINA   SE6   000
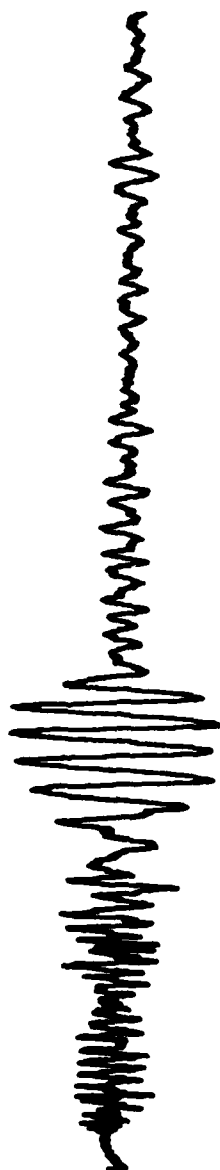
FONTINA   PAH   R

20 seconds

Figure 3-3:   Comparison of Seismograms Recorded at about the Same Epicentral
Distance Inside (SE-6) and Outside (PAH) the Las Vegas Valley

56

add coherently while, in general, energy traveling in other directions or at
other velocities will add incoherently and tend to cancel. Thus, the value of
ϕ for which a given arrival achieves maximum amplitude is associated with
the approach azimuth of the component of that arrival traveling with velocity C.

In the present application, since visual analyses of the seismograms
suggest that the reflected arrivals are predominantly Rayleigh waves with
periods ranging from only about 2.0 to 4.0 seconds, the simple beam-steer
process described above has been modified to take advantage of this additional
information (Murphy and O'Brien, 1978). Thus, since the arrivals of interest
are confined to a relatively narrow frequency band, the measured data are
filtered through an eighth order bandpass filter with a transfer function of
the form

$$T(S) = \left[\frac{\omega_c S}{S^2 + \omega_c S + \omega_c^2} \right]^4$$

where S is the Laplace transform variable and $\omega_c = 2\pi f_c$ with $f_c = 0.3\,Hz$.
This effectively eliminates shorter period body wave phases which are not
of interest in this study. Next, in order to isolate the Rayleigh waves
arriving from a selected approach azimuth ϕ, use is made of the fact
that the Rayleigh wave particle motion is restricted to the radial-vertical
plane oriented along the approach azimuth. That is, the radial component of
motion with respect to ϕ is computed by applying a rotation of axes to the
measured orthogonal, horizontal components of motion. Finally, the filtered
and rotated data from the array stations are summed with interstation time
delays appropriate for a plane wave approaching from direction ϕ at the
Raleigh wave velocity at 0.3 Hz.

In order to gain some insight into the response characteristics of
this set of filters, a simple example has been analyzed in which it was
assumed that the horizontal components of motion at the seven stations of
Figure 3-1 are the result of a superposition of two short duration synthetic

57

arrivals from different directions each consisting of four cycles of a
0.3 Hz sine wave. The first is taken to arrive on an azimuth from the source
(i.e., NTS) while the second arrives later from an azimuth of 140 degrees
with respect to the source and with delay times at each station appropriate
for the assumed Rayleigh wave velocity at a period of 3.0 seconds. The
results of applying the above defined filtering process to this set of
synthetic records are shown in Figure 3-4, for beam azimuths ranging from
0 to 360 degrees in 20 degree increments. It can be seen that the two
arrivals are clearly separated by this analysis procedure and that the
directions of approach and relative amplitudes of the two arrivals are
correctly identified. It appears that the angular resolution of this array
is approximately +20 degrees for the wavelengths of interest in this inves-
tigation.

The results of applying this filtering procedure to the CARPETBAG
data of Figure 3-2 are shown in Figure 3-5. In this figure, zero degrees
indicates the azimuth back toward the source and the angle is measured
clockwise from north. It can be seen that the output of the filter in this
case is remarkably consistent with that observed above in the case of the
simple example and clearly indicates some strong secondary bursts of energy
arriving from directions other than along the azimuth back to the source.
The strongest of these is an arrival originating at an azimuth between
160 and 180 degrees which propagates back up the line toward NTS. The general
amplitude level associated with this arrival is comparable to that of the direct,
suggesting that the reflection coefficient at the boundary which is the source
of this phase must be close to unity for incident Rayleigh waves with periods
near 3.0 seconds. The only other prominent secondary burst of energy which
can be easily identified in this figure is a still later arrival originating
at an azimuth of about 120 degrees which is quite similar in character to
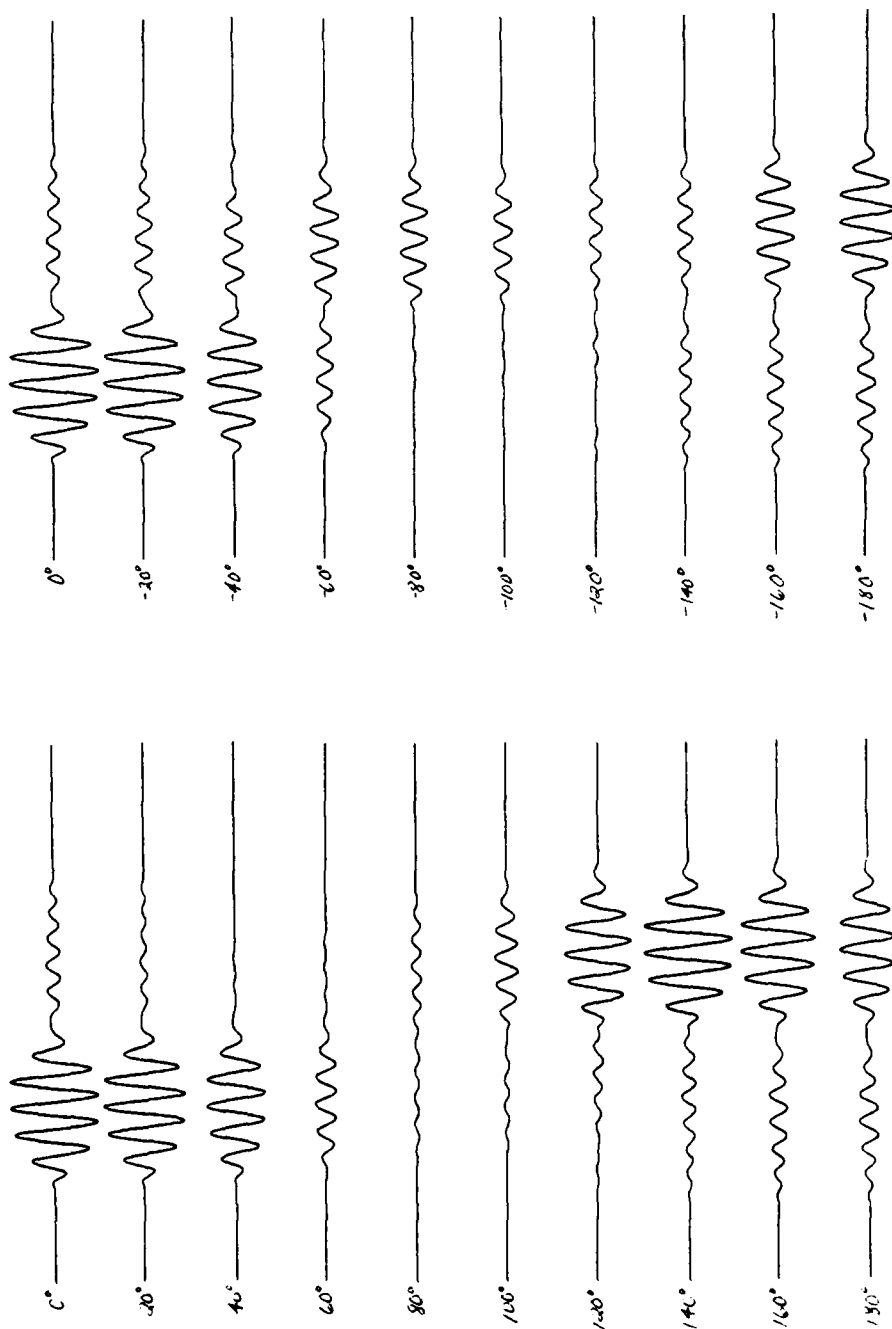that originating at 180 degrees.

Figure 3-4: Simulation of the Beam Steer Filtering Process
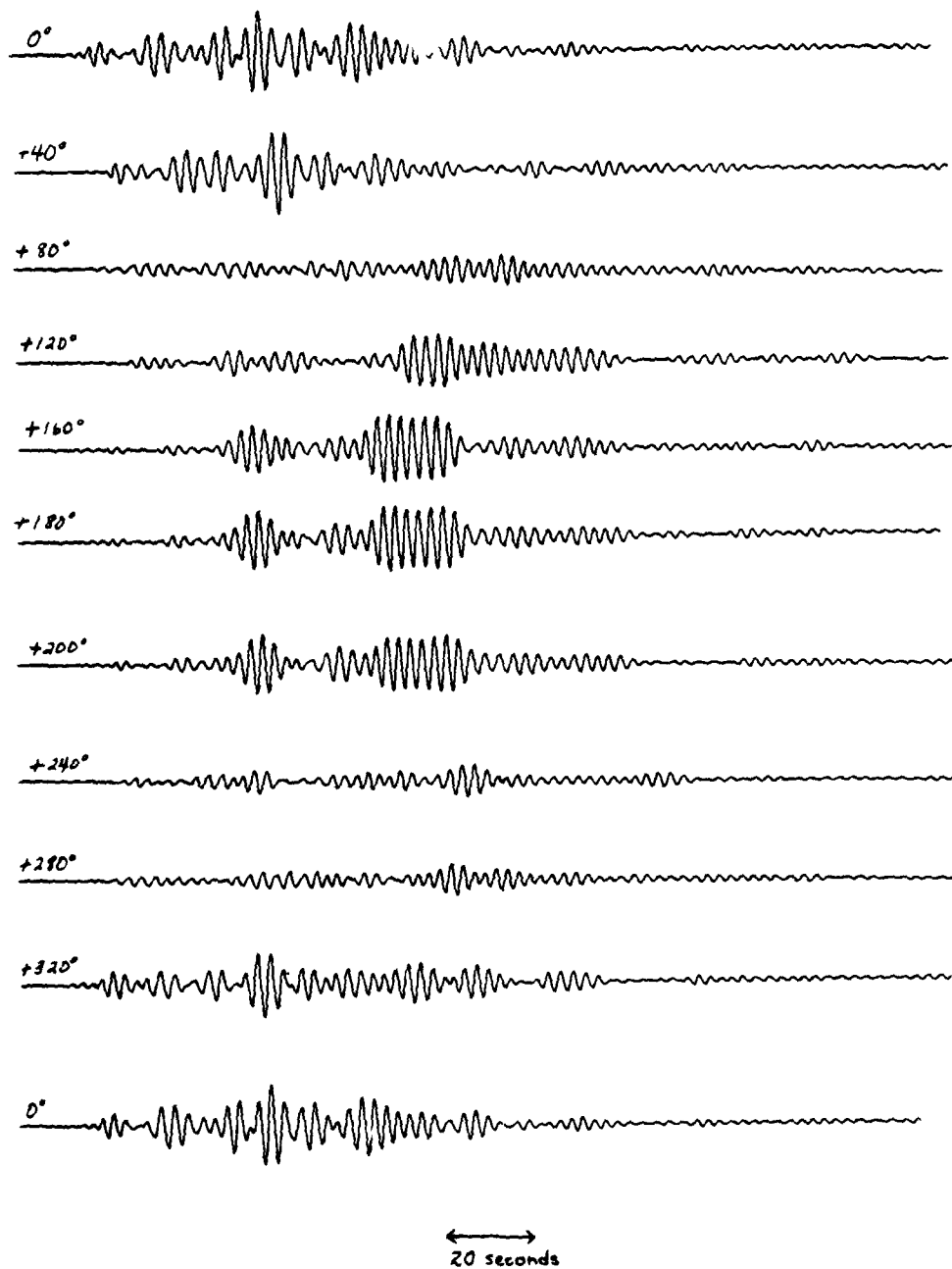
Figure 3-5: Beam Steer Analysis of the Carpetbag
Rayleigh Waves Recorded in Las Vegas

In order to complete the identification, it is necessary to correlate these arrivals with the structural boundaries of the valley. Figure 3-6 is a map of the Las Vegas Valley showing the locations of the surrounding mountain ranges with respect to the instrumentation array in Las Vegas. It can be seen that the valley is terminated in the southeast by the McCollough mountain range and, as is indicated by the arrow, the relative arrival time of the secondary signal from an azimuth of 180 degrees is consistent with it being a reflection from this boundary if the average Rayleigh wave propagation velocity at a period of 3.0 seconds is assumed. Perhaps even more interesting is the fact that the arrival time of the phase originating at an azimuth of 120 degrees is remarkably consistent with it being a multiply reflected arrival from Frenchman Mountain following the rather complicated path shown on this figure. If this latter identification is correct then this arrival must correspond to a fairly localized focusing of energy, since its amplitude seems to be too large to be consistent with the hypothesized non-planar reflection. Unfortunately, the subsurface geology in the vicinity of these valley boundaries is not well known and, consequently, it is not possible to formulate a quantitative model of the reflection process at the present time. However, it is known that the alluvium gradually thins with distance from the valley center and that the underlying Paleozoic rocks are abruptly terminated by the valley boundary faults giving rise to a discontinuity in physical properties which could produce a strong reflection. Moreover, due to the gradual thinning of the alluvial layer, components of the incident signal of different wavelengths can be expected to exhibit different reflection coefficient characteristics. Thus, only a selected band of frequencies would be expected to be strongly reflected, in agreement with the narrowband character of the reflected signals.

Figure 3-6: Las Vegas Valley Map Showing Approximate Travel Paths of Secondary Surface Wave Arrivals in Las Vegas

3.3 Analysis of Yucca Valley Data
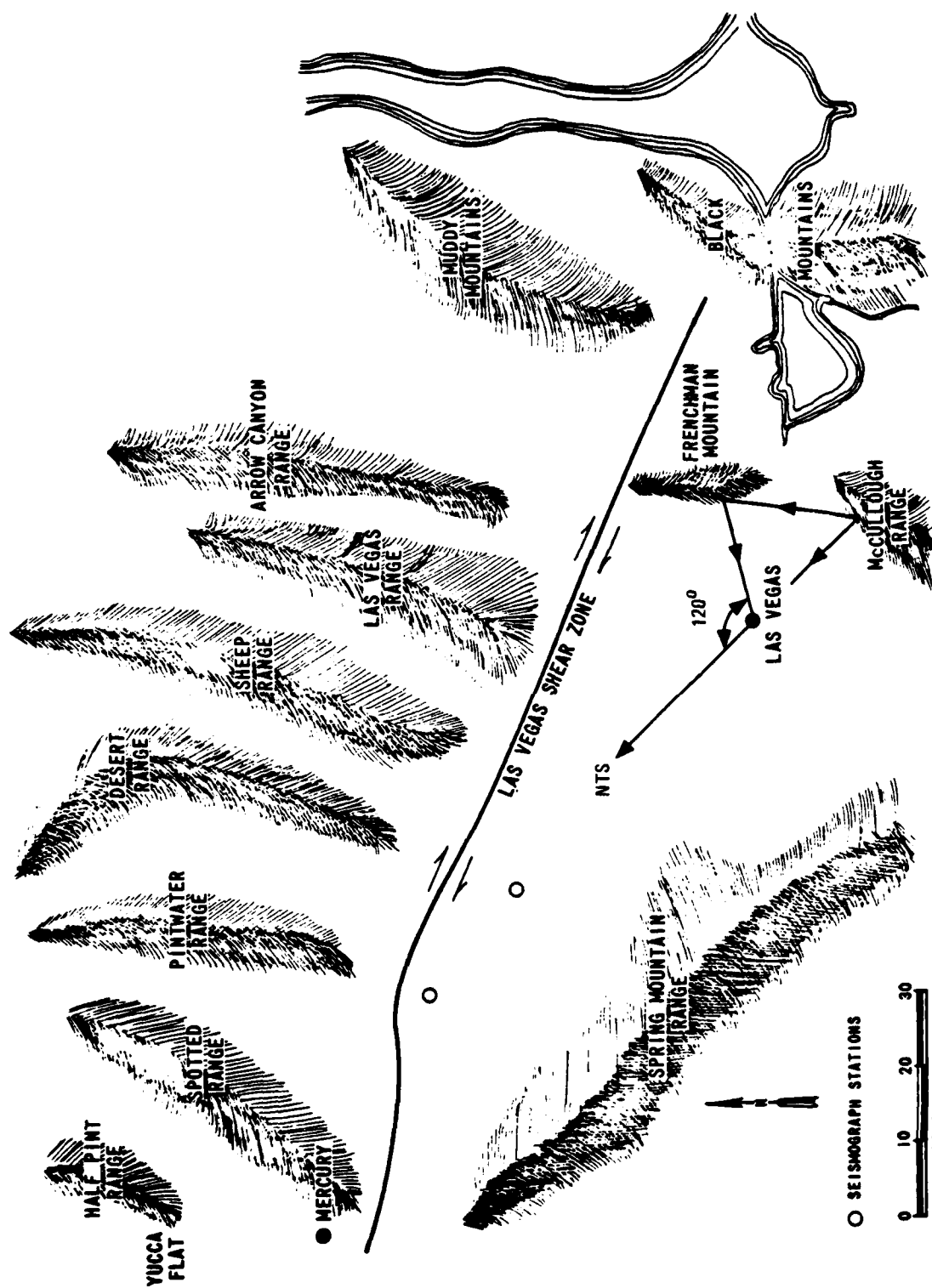
The Las Vegas data analysis presented above clearly illustrates the fact that the presence of the valley boundaries can significantly modify the ground motion experienced in the valley. However, it is not directly relevant to the MX valley reverberation question in that the source was located some 150 km away outside of the valley. In order to examine the problem on a more appropriate scale, data recorded from the NTS event CALABASH in Yucca Valley have also been analyzed. Figure 3-7 shows the locations of CALABASH and the stations that were deployed to measure the near-field ground motions from this event. It can be seen from this figure that the instrumentation array encompasses stations located at about the same distance (7 to 8 km) both outside and inside the valley. Figure 3-8 shows a vertical subsurface geologic section through the line A-A' on Figure 3-7 which indicates that the alluvium gradually thins to the west until it terminates against the underlying tuff formation at the valley boundary. Figure 3-9 shows a comparison of the CALABASH radial component velocity time histories measured at stations 752 (in the valley) and 755 (on the valley boundary). It can be seen that although these stations are located at about the same distance from the source, there is a significant difference in the effective duration with the closer, in-valley station (752) showing clear evidence of later secondary arrivals. This difference is even more apparent when the envelopes of the signals in a narrow frequency band are compared. Figure 3-10 shows a block diagram of the envelope detector which was selected to process the recorded data. The passband around 1 Hz was chosen for analysis in this case on the basis of a visual identification of the characteristic frequencies of the late-time motions recorded on the array. Figure 3-11 shows the 1 Hz envelopes of the signals shown in Figure 3-9 and Figure 3-12 shows the envelopes for another pair of stations one of which is inside (746) and one
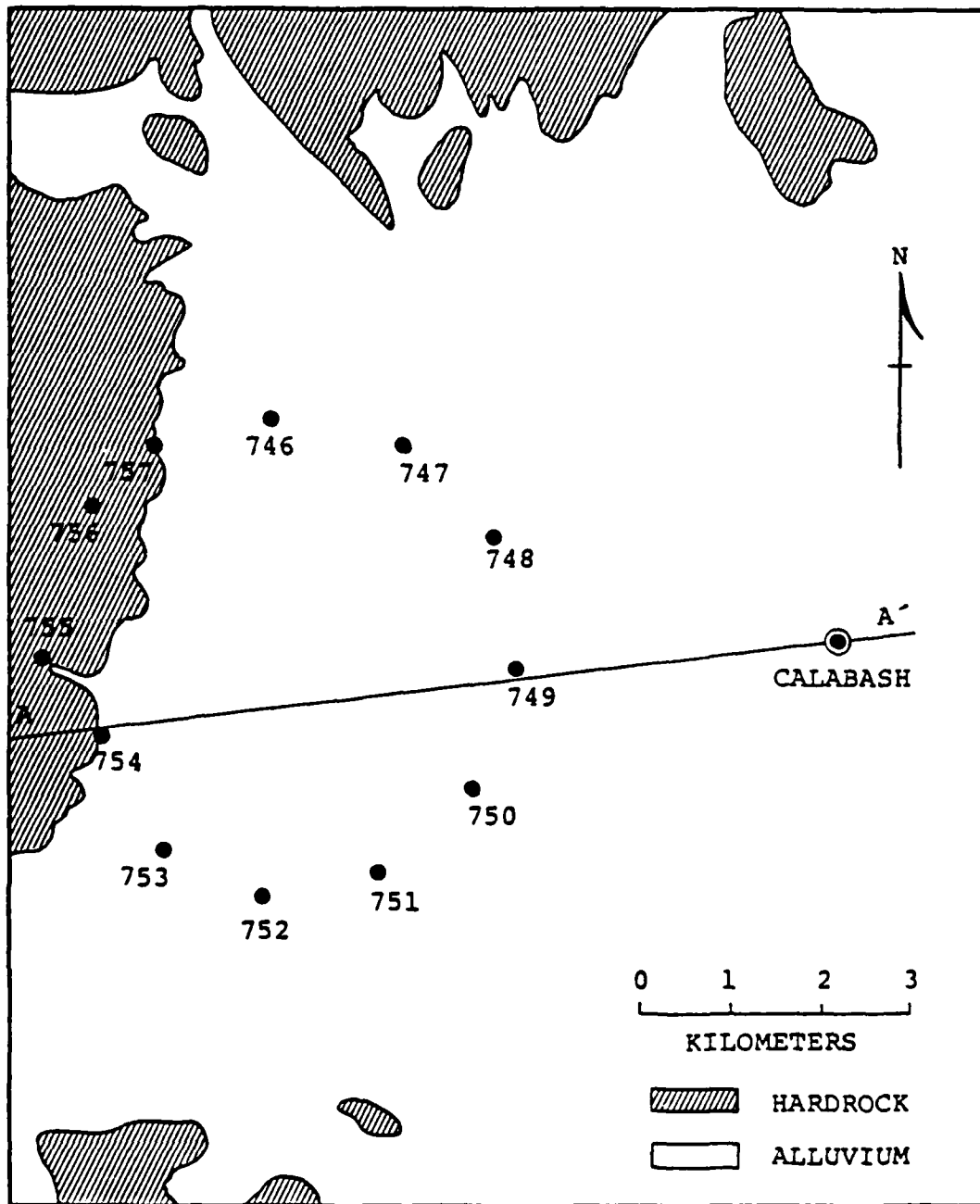
Figure 3-7:   Calabash Station Location Map
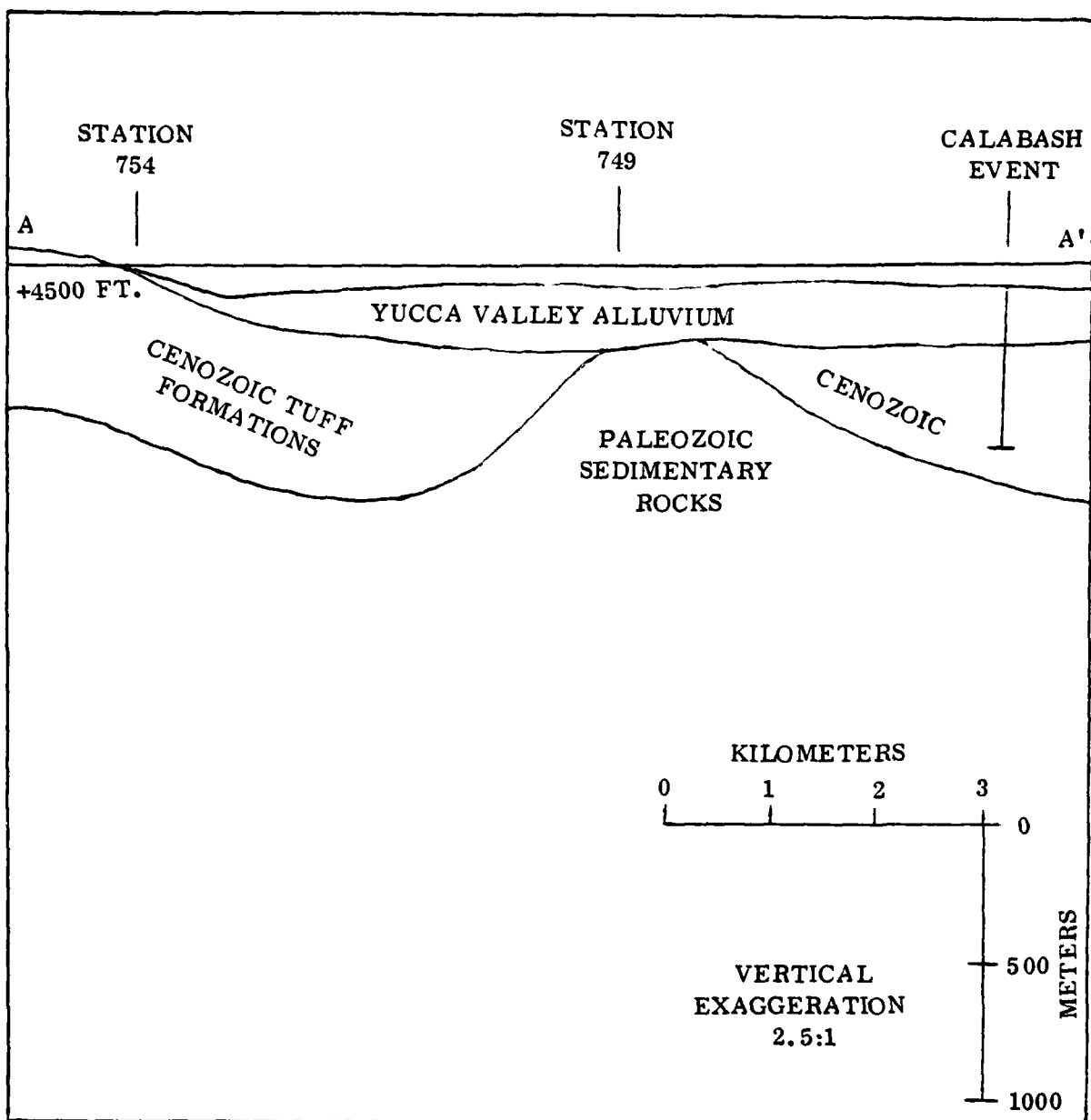
Figure 3-8: Vertical Geologic Section for the Calabash Event
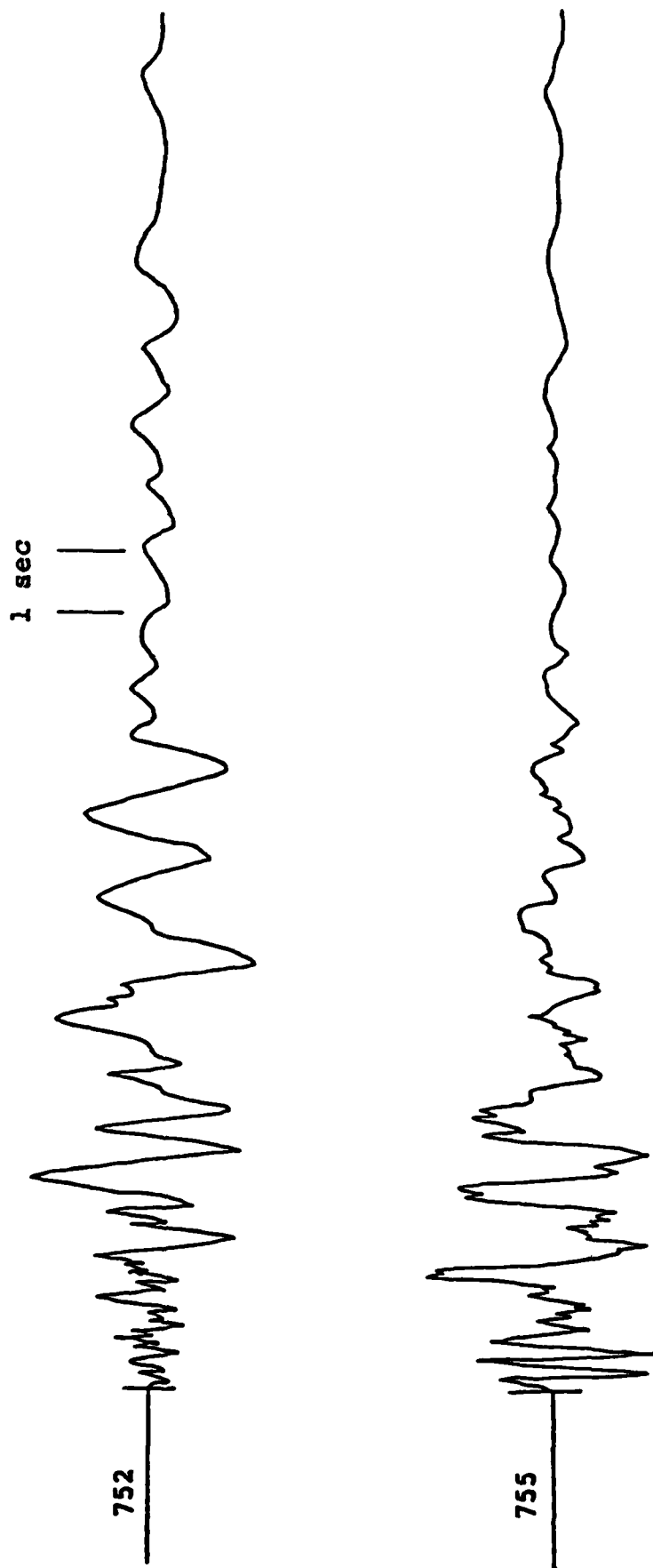
Figure 3-9: Comparison of Ground Motion Records Recorded at about the Same Distance Inside (752) and Outside (755) Yucca Valley, Calabash Event

66
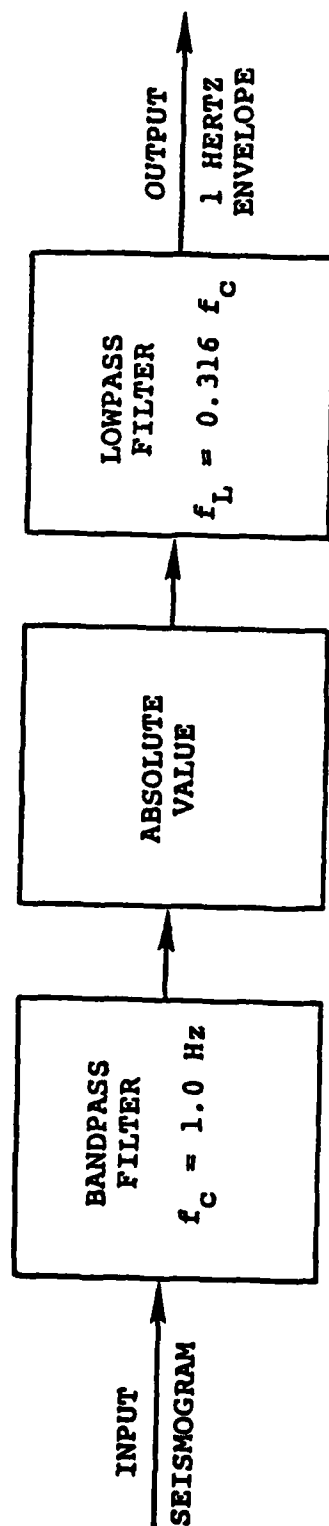
Figure 3.10: Block Diagram of Envelope Circuit
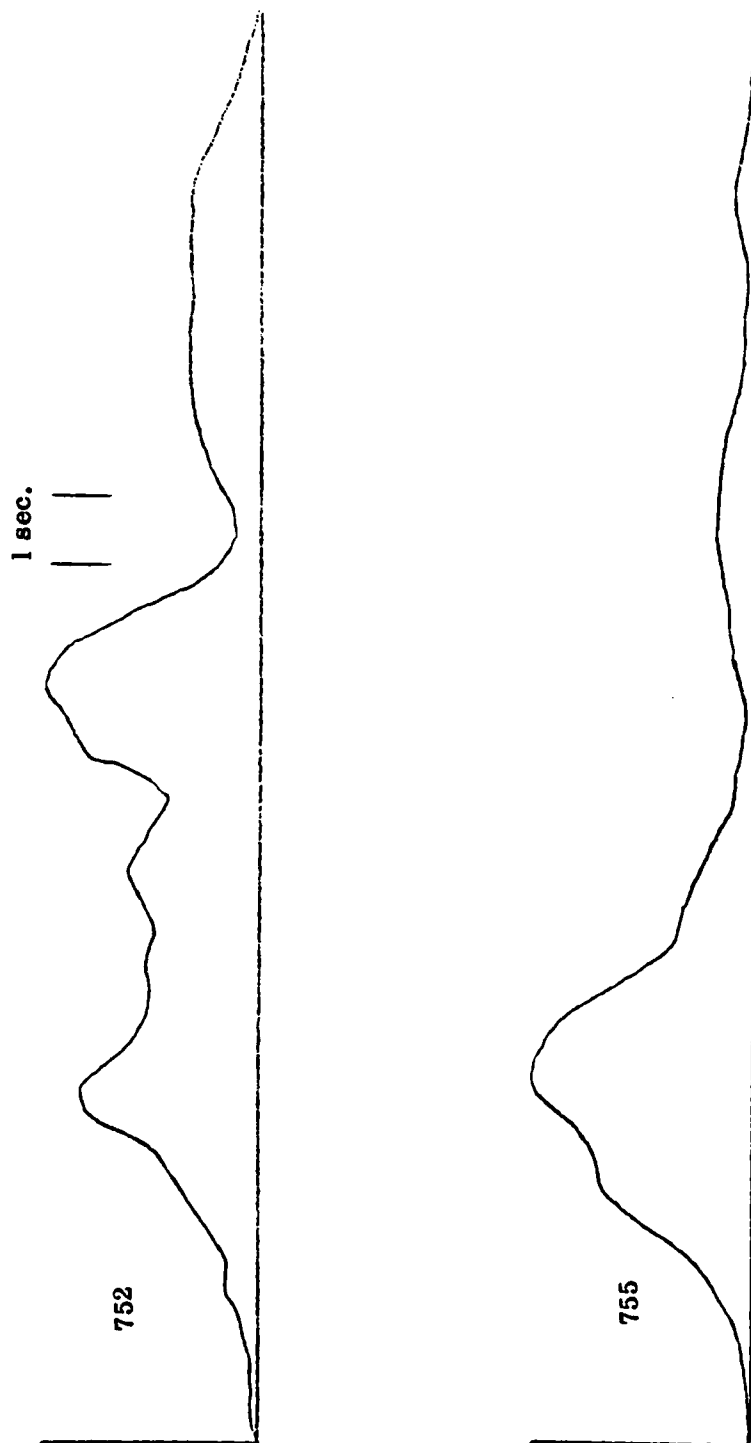
Figure 3-11: Comparison of the One Hertz Envelope for Stations
Inside (752) and Outside (755) Yucca Valley
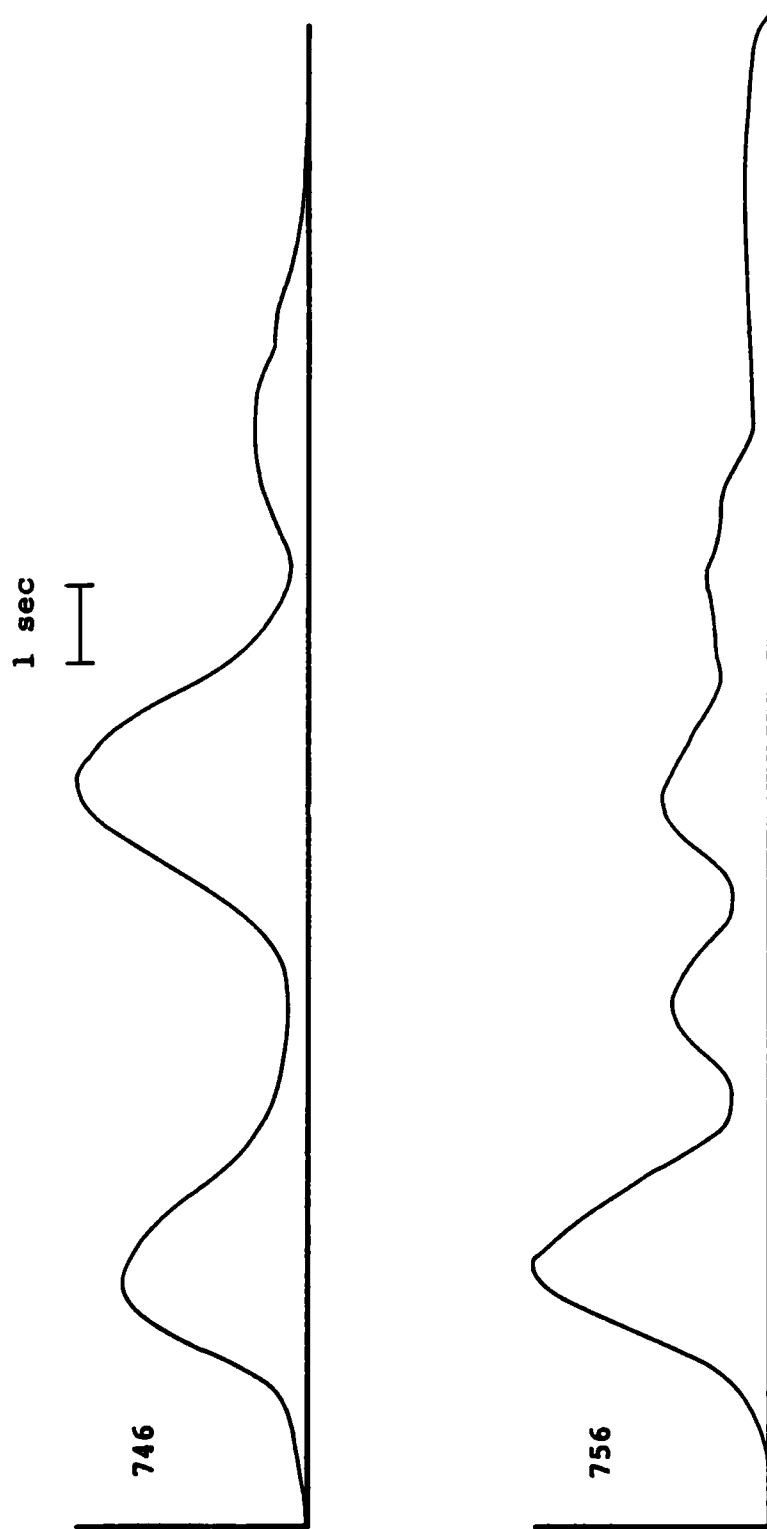
Figure 3.12: Comparison of the One Hertz Envelope for Stations Inside (746) and Outside (756) Yucca Valley

of which is outside (756) the valley. In both cases there is clear evidence

of strong secondary arrivals at the stations inside the valley which appear

to have no counterparts on the records of adjacent stations located outside

the valley. This strongly suggests that a significant amount of energy

is being reflected back from the valley boundary and modifying the motion

inside the valley.

3.4   Conclusions

Preliminary analyses of NTS seismic data recorded in two different

valley structures have confirmed that the presence of the valley boundaries

can significantly modify the ground motion environment within the valley.

This appears to be particularly true for the late-time, low frequency

components of the motion. More specifically, in both the cases analyzed in

this study, the arrivals identified as reflections from the valley boundaries

have been found to be comparable in amplitude to the corresponding direct

arrivals, suggesting that the reflection coefficients at such boundaries can

be close to unity in particular frequency bands of interest. Thus, the

empirical data suggest that valley reverberation may have a pronounced

influence on the late-time ground motion environment for MX. More detailed

investigations will be required before the magnitude of this effect can

be confidently estimated.

Chapter 4

Summary and Recommendations for Further Study

The investigation summarized in this report has centered on an attempt to develop an improved, quantitative understanding of the late-time, oscillatory components of the ground motions observed from surface explosions. This effort has encompassed studies of the source and mode of propagation associated with these arrivals as well as some preliminary investigations of the effect of surrounding geologic boundaries on the late-time ground motion environment to be expected at sites located in intermontane valleys.

In Chapter 2 a theoretical model was described which can be used to compute the surface waves produced by a propagating airblast load acting on the surface of a multilayered, elastic halfspace. This model was then applied to the analysis of both the observed data and finite difference simulations of the Pre-Mine Throw and Pre-Dice Throw 100 ton HE surface bursts. As a result of this analysis, the observed late-time, oscillatory components of the ground motion have been conclusively identified as classical, Rayleigh-type surface waves. Moreover, it has been found that the observed surface wave data from the PMT and PDT explosions can be matched surprisingly well with respect to both frequency content and absolute amplitude level by considering only the airblast induced elastic motions originating at ranges greater than about 11 m from ground zero. This has been interpreted as an indication that the loading inside of this radius may not be efficiently coupled into radiated surface waves due to energy losses associated with crater formation and other nonlinear interactions which are known to take place in the vicinity of ground zero. Thus, it appears that it may be possible to estimate the oscillatory Rayleigh wave components of the ground motion from surface explosions using relatively simple approximations to the seismic source function.

71

Some preliminary analyses of the valley reverberation phenomenon were summarized in Chapter 3. Ground motion data recorded in Yucca Valley on NTS and in the Las Vegas Valley approximately 150 km SE of NTS were studied using a variety of signal processing techniques. These studies have confirmed the fact that the presence of the valley boundaries can significantly modify the late-time, low frequency ground motion environment within the valley. More specifically, in both cases the arrivals identified as reflections from the valley boundaries were found to be comparable in amplitude to the corresponding direct arrivals, suggesting that the reflection coefficients at such boundaries can be close to unity in particular frequency bands of interest.

On the basis of the results described above, it is clear that additional research is needed in both study areas. With regard to the surface wave studies, it is recommended that additional research be performed with the objective of defining the uniqueness and physical significance of the airblast loading approximation which was found to account for the observed surface wave data from the PMT and PDT explosions. It is further recommended that the analytic surface wave model be incorporated into a procedure for providing a firmer, quantitative basis for scaling to new geologic environments and source conditions.

With regard to the valley reverberation investigation, there are at least three Yucca Valley arrays, in addition to CALABASH, that were recorded on broad-band magnetic tape instruments and that appear, from a preliminary examination, to show evidence of valley reverberation effects. It is recommended that more detailed analyses be made of these data to identify the source of late-arriving seismic signals and to quantify their amplitude levels relative to the early direct arrivals. Also, data have been collected on several specially designed instrumentation arrays which were deployed on the MISERS BLUFF II series of HE tests recently conducted at the Planet Ranch

Site in Arizona. It is recommended that these data be carefully analyzed and used both to formulate an approximate surface wave synthesis model and to verify valley reverberation effects.

References

Auld, H. E., D. Mason and C. J. Higgins, 1978, "Pre-Dice Throw II - 1 and Pre-Mine Throw IV - 6 Elastic Calculations", Report to Air Force Weapons Laboratory, January, 1978.

Auld, H. E. (1978), University of New Mexico, Civil Engineering Research Facility, Private Communication.

Ewing, W. M., W. S. Jardetzky and Frank Press, 1957, Elastic Waves in Layered Media, McGraw-Hill Book Company, Inc., New York.

Harkrider, D. G. 1964, "Surface Waves in Multilayered Elastic Media I. Rayleigh and Love Waves From Buried Sources in a Multilayered Elastic Half-Space." Bulletin of the Seismological Society of America, vol. 54, pp 627-679.

Harkrider, D. G., C. A. Newton and E. A. Flinn, 1974 "Theoretical Effect of Yield and Burst Height of Atmospheric Explosions on Rayleigh Wave Amplitudes" Geophysical Journal of the Royal Astronomical Society, vol. 36, pp 191-225.

Haskell, N. A., 1953, " The Dispersion of Surface Waves in Multilayered Media" Bulletin of the Seismological Society of America, vol. 43, pp 17-34.

Murphy, J. R. and R. A. Hewlett, 1975, "Analysis of Seismic Response in the City of Las Vegas, Nevada: A Preliminary Microzonation", Bulletin of the Seismological Society of America, vol. 65, pp 1575-1597.

Murphy, J. R. and L. J. O'Brien, 1978, "An Investigation of the Reflection of Short-Period Surface Waves From Valley Boundaries", Paper presented at the Annual Meeting of the Seismological Society of America, April, 1978.

DISTRIBUTION LIST

DEPARTMENT OF DEFENSE

Assistant to the Secretary of Defense
Atomic Energy
    ATTN: Executive Assistant

Defense Advanced Rsch Proj Agency
    ATTN: TIO

Defense Intelligence Agency
    ATTN: RDS-3A

Defense Nuclear Agency
    ATTN: SPSS, J. Galloway
 2 cy ATTN: SPSS, G. Ullrich
 4 cy ATTN: TITL

Defense Technical Information Center
12 cy ATTN: DD

Field Command
Defense Nuclear Agency
    ATTN: FCTMD
    ATTN: FCPR

Field Command
Defense Nuclear Agency
Livermore Division
    ATTN: FCPRL

Joint Strat Tgt Planning Staff
    ATTN: XPFS
    ATTN: NRI-STINFO Library

Undersecretary of Def for Rsch & Engrg
Department of Defense
    ATTN: Strategic & Space Systems (OS)

DEPARTMENT OF THE ARMY

BMD Advanced Technology Center
    ATTN: ATC-T

Chief of Engineers
Department of the Army
    ATTN: DAEN-MPE-T, D. Reynolds
    ATTN: DAEN-RDM
    ATTN: DAEN-RDL
    ATTN: DAEN-ASI-L

Harry Diamond Laboratories
Department of the Army
    ATTN: DELHD-N-P
    ATTN: DELHD-I-TL

U.S. Army Ballistic Research Labs
    ATTN: DRDAR-TSB-S
    ATTN: DRDAR-BLE, J. Keefer

BMD Systems Command
Department of the Army
    ATTN: BMDSC-HW

U.S. Army Cold Region Res Engr Lab
    ATTN: Library

DEPARTMENT OF THE ARMY (Continued)

U.S. Army Construction Engr Res Lab
    ATTN: Library

U.S. Army Engineer Center
    ATTN: Technical Library

U.S. Army Engr Waterways Exper Station
    ATTN: WESSD, G. Jackson
    ATTN: Library
    ATTN: WESSA, W. Flathau
    ATTN: J. Zelasko

U.S. Army Material & Mechanics Rsch Ctr
    ATTN: Technical Library

U.S. Army Materiel Dev & Readiness Cmd
    ATTN: DRXAM-TI

U.S. Army Nuclear & Chemical Agency
    ATTN: Library
    ATTN: T. Simms

DEPARTMENT OF THE NAVY

Naval Construction Battalion Center
Civil Engineering Laboratory
    ATTN: Code L08A
    ATTN: Code L51, J. Crawford
    ATTN: Code L53, J. Forrest

Naval Facilities Engineering Command
    ATTN: Code 09M22C

Naval Postgraduate School
    ATTN: Code 0142 Library
    ATTN: G. Lindsay

Naval Research Laboratory
    ATTN: Code 2627

Naval Surface Weapons Center
    ATTN: Code X211
    ATTN: Code F31

Naval Surface Weapons Center
    ATTN: Tech Library & Info Services Branch

Office of Naval Research
    ATTN: Code 715

DEPARTMENT OF THE AIR FORCE

Air Force Institute of Technology
    ATTN: Library

Air Force Systems Command
    ATTN: DLWM

DEPARTMENT OF THE AIR FORCE (Continued)

Air Force Weapons Laboratory
Air Force Systems Command
        ATTN: NTE, M. Plamondon
        ATTN: SUL
        ATTN: NT, D. Payton
        ATTN: NTED-I
        ATTN: NTED-A
        ATTN: DEY
        ATTN: NTES-S
        ATTN: NTES-G
        ATTN: NTEO

Assistant Chief of Staff
Intelligence
Department of the Air Force
        ATTN: IN

Research, Development & Logistics
Department of the Air Force
        ATTN: SAFALR/Dep for Strat & Space Sys

Ballistic Missile Office
Air Force Systems Command
        ATTN: MNNX, W. Crabtree
        ATTN: MNNXH, D. Gage

Research, Development & Acq
Department of the Air Force
        ATTN: AFRDQA
        ATTN: AFRDPN
        ATTN: AFRDQSM
        ATTN: AFRD-P, N. Alexandrow

Strategic Air Command
Department of the Air Force
        ATTN: NRI-STINFO Library
        ATTN: XPFS

Vela Seismology Center
        ATTN: G. Ullrich

DEPARTMENT OF ENERGY CONTRACTORS

Lawrence Livermore National Laboratory
        ATTN: D. Glenn

Los Alamos National Scientific Lab
        ATTN: R. Sanford
        ATTN: C. Keller

Sandia National Laboratories
        ATTN: A. Chabai
        ATTN: Org 1250, W. Brown

DEPARTMENT OF DEFENSE CONTRACTORS

Acurex Corp
        ATTN: K. Triebes
        ATTN: C. Wold
        ATTN: J. Stockton

Aerospace Corp
        ATTN: Technical Info Services
        ATTN: H. Mirels

Agbabian Associates
        ATTN: M. Agbabian

DEPARTMENT OF DEFENSE CONTRACTORS (Continued)

Applied Theory, Inc
  2 cy ATTN: J. Trulio

Boeing Company
        ATTN: Aerospace Library
        ATTN: S. Strack

ARTEC Associates, Inc
        ATTN: S. Gill

California Research & Technology, Inc
        ATTN: M. Rosenblatt
        ATTN: Library

Civil Systems, Inc
        ATTN: S. Melzer

Eric H. Wang
Civil Engineering Rsch Fac
University of New Mexico
        ATTN: J. Kovarna
        ATTN: P. Lodde
        ATTN: J. Lamb

General Electric Company—TEMPO
        ATTN: DASIAC

University of Denver
Colorado Seminary
        ATTN: J. Wisotski

H-Tech Labs, Inc
        ATTN: B. Hartenbaum

Higgins, Auld & Associates
        ATTN: H. Auld
        ATTN: N. Higgins
        ATTN: J. Bratton

IIT Research Institute
        ATTN: Documents Library

J. H. Wiggins Company, Inc
        ATTN: J. Collins

Kaman AviDyne
        ATTN: R. Ruetenik

Merritt CASES, Inc
        ATTN: Library

Mission Research Corp
        ATTN: C. Longmire
        ATTN: G. McCartor

Nathan M. Newmark Consult Eng Svcs
        ATTN: W. Hall
        ATTN: N. Newmark

Pacific-Sierra Research Corp
        ATTN: H. Brode

Pacifica Technology
        ATTN: R. Allen
        ATTN: Library

76

Physics International Company
    ATTN: Technical Library
    ATTN: F. Sauer
    ATTN: J. Thomsen

R & D Associates
    ATTN: J. Lewis
    ATTN: Technical Information Center
    ATTN: C. MacDonald
    ATTN: R. Port
    ATTN: J. Carpenter
    ATTN: P. Haas
    ATTN: A. Kuhl

Science Applications, Inc
    ATTN: R. Schlaug
    ATTN: Technical Library
    ATTN: H. Wilson

Science Applications, Inc
    ATTN: D. Houe

Science Applications, Inc
    ATTN: B. Chambers III

SRI International
    ATTN: D. Johnson
    ATTN: J. Colton
    ATTN: G. Abrahamson
    ATTN: Library

Weidlinger Assoc, Consulting Engineers
    ATTN: J. Isenberg

Systems, Science & Software, Inc
    ATTN: C. Needham

Systems, Science & Software, Inc
    ATTN: Library
    ATTN: K. Pyatt
    ATTN: J. Barthel

Systems, Science & Software, Inc
    ATTN: J. Murphy

Systems, Science & Software, Inc
    ATTN: C. Hastings

Terra Tek, Inc
    ATTN: A. Abou-Sayed
    ATTN: Library

TRW Defense & Space Sys Group
    ATTN: Technical Information Center
    ATTN: N. Lipner
    ATTN: T. Mazzola

TRW Defense & Space Sys Group
    ATTN: G. Hulcher

Weidlinger Assoc, Consulting Engineers
    ATTN: I. Sandler